Article

Current Biology

Extrasynaptic signaling enables an asymmetric juvenile motor circuit to produce symmetric undulation

Graphical abstract

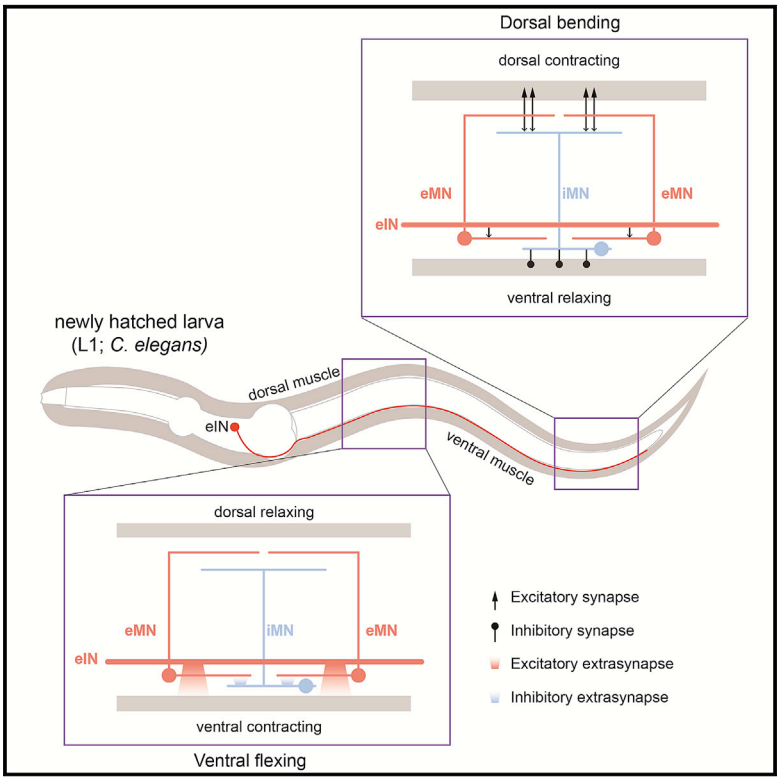

Highlights

- *C. elegans* larvae generate symmetric motor output with asymmetric motor circuit
- Dorsal bending by synaptic wiring between excitatory and inhibitory motor neurons
- Tonic extrasynaptic ventral muscle excitation by cholinergic premotor interneurons
- Ventral bending generated by anti-phasic entrainment of the dorsal bending circuit

Authors

Yangning Lu, Tosif Ahamed, Ben Mulcahy, ..., Andrew D. Chisholm, Aravinthan D.T. Samuel, Mei Zhen

Correspondence

meizhen@lunenfeld.ca

In brief

A newborn worm's motor circuit is asymmetric, wired to only make dorsal bends. However, they make dorsoventral undulations. Lu et al. show that ventral bends happen by a tonic potentiation of ventral muscles by cholinergic premotor interneurons and anti-phasic entrainment to the dorsal bends.

Lu et al., 2022, Current Biology *32*, 4631–4644
November 7, 2022 Crown Copyright © 2022 Published by Elsevier Inc.
https://doi.org/10.1016/j.cub.2022.09.002

Current Biology

CellPress

Article

Extrasynaptic signaling enables an asymmetric juvenile motor circuit to produce symmetric undulation

Yangning Lu,[1,2,7,8,11] Tosif Ahamed,[2,7,12] Ben Mulcahy,[2] Jun Meng,[1,2] Daniel Witvliet,[2,3,9] Sihui Asuka Guan,[1,2,10] Douglas Holmyard,[2] Wesley Hung,[2] Quan Wen,[4,5] Andrew D. Chisholm,[6] Aravinthan D.T. Samuel,[4] and Mei Zhen[1,2,3,13,14,*]

[1]Department of Physiology, University of Toronto, Toronto, ON M5G 1X5, Canada
[2]Lunenfeld-Tanenbaum Research Institute, Mount Sinai Hospital, Toronto, ON M5G 1X5, Canada
[3]Department of Molecular Genetics, University of Toronto, Toronto, ON M5G 1X5, Canada
[4]Department of Physics and Center for Brain Science, Harvard University, Cambridge, MA 02138, USA
[5]School of Life Sciences, University of Science and Technology, Hefei, Anhui 230027, China
[6]Division of Biological Sciences, University of California, San Diego, La Jolla, CA 92093, USA
[7]These authors contributed equally
[8]Current address: McGovern Institute for Brain Research, Massachusetts Institute of Technology, Cambridge, MA 02139, USA
[9]Current address: Coursera, Toronto, ON M5C 2L7, Canada
[10]Current address: Overland Pharmaceuticals Inc., Jing'an District, Shanghai 20070, China
[11]Twitter: @YangningL
[12]Twitter: @_mlechha
[13]Twitter: @zhenlab_Toronto
[14]Lead contact
*Correspondence: meizhen@lunenfeld.ca
https://doi.org/10.1016/j.cub.2022.09.002

SUMMARY

In many animals, there is a direct correspondence between the motor patterns that drive locomotion and the motor neuron innervation. For example, the adult *C. elegans* moves with symmetric and alternating dorsal-ventral bending waves arising from symmetric motor neuron input onto the dorsal and ventral muscles. In contrast to the adult, the *C. elegans* motor circuit at the juvenile larval stage has asymmetric wiring between motor neurons and muscles but still generates adult-like bending waves with dorsal-ventral symmetry. We show that in the juvenile circuit, wiring between excitatory and inhibitory motor neurons coordinates the contraction of dorsal muscles with relaxation of ventral muscles, producing dorsal bends. However, ventral bending is not driven by analogous wiring. Instead, ventral muscles are excited uniformly by premotor interneurons through extrasynaptic signaling. Ventral bends occur in anti-phasic entrainment to activity of the same motor neurons that drive dorsal bends. During maturation, the juvenile motor circuit is replaced by two motor subcircuits that separately drive dorsal and ventral bending. Modeling reveals that the juvenile's immature motor circuit is an adequate solution to generate adult-like dorsal-ventral bending before the animal matures. Developmental rewiring between functionally degenerate circuit solutions, which both generate symmetric bending patterns, minimizes behavioral disruption across maturation.

INTRODUCTION

Many animals generate alternating motor patterns that are thought to reflect similar motor neuron input. *C. elegans* generates alternating dorsal-ventral bending waves for locomotion.[1] The wiring diagram of its adult motor circuit contains similar inputs, from both excitatory motor neurons (eMNs) and inhibitory motor neurons (iMNs), onto both dorsal and ventral body wall muscles.

The adult *C. elegans* motor system consists of two homologous motor neuron networks.[2,3] In this circuit, dorsal and ventral muscles form neuromuscular junctions (NMJs) with two sets of cholinergic eMNs that contract muscles, as well as with two sets of GABAergic iMNs that relax muscles.[4–6] NMJs from eMNs are also dyadic synapses to the iMNs that form NMJs with muscles on the opposite side, thus coordinating muscle contraction and relaxation.

One motor subcircuit consists of repeated modules of cholinergic eMNs (DA and DB) and GABAergic iMNs (VD). They coordinate simultaneous dorsal muscle contraction and ventral muscle relaxation in each body segment, producing dorsal bends. A complementary motor subcircuit produces ventral bends, with symmetric wiring of a homologous set of eMNs (VA and VB) and iMNs (DD).[3] Integrating the role of oscillators and proprioceptors, eMNs underlie rhythmic and coordinated body bending.[7–12] Alternating activity of these two subcircuits in each body segment gives rise to alternating dorsal and ventral bending during adult locomotion.[13]

However, the newly born larva (L1) lacks this symmetry. For the first few hours after birth, an L1 larva has only the DA, DB, and DD motor neurons.[14] A partial electron microscopy (EM) reconstruction of the L1 larva[2] suggests that its motor neuron wiring is different from that in the adult:[3] DA and DB make NMJs exclusively to dorsal muscles, and DD make NMJs exclusively to ventral muscles. NMJs from DA and DB are also dyadic synapses to the DD. Hence, the entire L1 wiring resembles an adult's subcircuit for dorsal bending.

Despite lacking a homologous motor circuitry to drive ventral bends, the L1 larva crawls with an adult-like undulation. Here, combining EM reconstruction, functional imaging, optogenetic perturbation, cell and synapse ablation, and modeling, we resolved mechanisms by which the L1's structurally asymmetric motor circuit produces a motor pattern with dorsal-ventral symmetry.

RESULTS

L1 motor neurons have asymmetric input to dorsal and ventral body wall muscles

C. elegans are born with a fraction of motor neurons of the adult motor circuit. Beginning at the mid-L1 larva stage, post-embryonic neurogenesis gives rise to new motor neurons.[15] Because all motor neurons that innervate ventral muscles in adults are born post-embryonically,[3] the L1 larva motor neurons must have a distinct and potentially asymmetrically wired configuration.

We used serial section EM to fully reconstruct the motor circuit of multiple L1 larvae, from premotor interneurons to motor neurons to muscles (Mulcahy et al., 2022;[16] this study). In an early L1 larva (Figures 1 and S1), we confirmed results for motor neurons from a previous partial reconstruction:[2] inputs to dorsal and ventral muscles are asymmetric (Figure 1B). All cholinergic eMNs (DA and DB) make NMJs only to dorsal muscles. All GABAergic iMNs (DD) make NMJs only to ventral muscles. Most NMJs from the eMNs are dyadic, innervating dorsal muscles as well as the iMNs that project to the opposite side (Figure S1). Multiple eMNs and iMNs (Figure 1A) form a chain of similarly wired modules along the body (Figure 1B).

In the adult motor circuit, two different groups of eINs (premotor interneurons) innervate the A- and B-class eMNs to regulate directional movements.[13,17] Our EM reconstruction revealed that this wiring pattern is already present in the newborn L1 larva (Figures 1 and S1; Mulcahy et al., 2022[16]). The DA subclass of eMNs is postsynaptic to cholinergic eINs that regulate backward locomotion (AVA, AVE, and AVD); the DB subclass of eMNs are postsynaptic to eINs that promote forward locomotion (AVB and PVC). Thus, the key differences in structural wiring between the L1 and adult motor circuits are the motor neurons and their connections to muscles.

L1 larvae generate dorsal-ventral alternating body bends and muscle activities

Despite dorsal and ventral muscles receiving asymmetric inputs, *C. elegans*'s alternating dorsal-ventral bending pattern is established at birth. When swimming, L1 larvae exhibited sinusoidal bending waves and full-body coils without dorsal or ventral bias (Figure 1C; Video S1A). When crawling, L1 larvae propagated alternating, dorsal-ventral bending waves along the body (Figures 1D and 1E; Video S1B).

The calcium dynamics of body wall muscles[18] correlated with this bending pattern. In slowly crawling L1 larvae (Video S1C), calcium waves propagated along dorsal and ventral muscles and tracked curvature changes (Figures 1D and 1E). Consistently, dorsal-ventral alternation in body bending correlated with out-of-phase activation of the corresponding muscles (Figures 1D and 1E). Overall, dorsal and ventral muscle activity level is balanced.

Wiring asymmetry of the L1 motor circuit needs to be reconciled with the bending symmetry. We began with determining the functional relationship between each class motor neurons with bending.

Cholinergic eMNs drive dorsal muscle contraction

When L1 larvae moved backwards, DA motor neurons were activated in retrograde sequence as bending traveled from tail to head (Figure 2A; Video S2A). Calcium dynamics at each DA soma correlated with dorsal bending, exhibiting the shortest time lag with bending of the anterior body segment (Figure 2A). This position-dependent correlation is consistent with the anatomical wiring: DA axons project anteriorly, making exclusive NMJs to dorsal muscles anterior to their somas (Figure 1B).

When L1 larvae moved forward, DB motor neurons were activated in an anterograde sequence (Figure 2B; Video S2B). Calcium dynamics at each DB soma correlated with dorsal bending, exhibiting the shortest time lag with bending of the posterior body segment (Figure 2B), consistent with the posterior projection of DB axons (Figure 1B). These results establish positive correlations between eMNs and dorsal bending.

Activation of all eMNs by Chrimson[20] increased calcium activity of dorsal muscles, but not ventral muscles (Figure 2C). Inhibition of eMNs by GtACR2[21] lowered the activity of dorsal muscles but led to an activity increase in ventral muscles (Figure 2D). Cholinergic inputs from eMNs are excitatory specifically to dorsal muscles.

GABAergic iMNs promote ventral and dorsal muscle relaxation

GABAergic motor neurons (DD) make NMJs exclusively to ventral muscles. Each DD makes a cluster of NMJs as an imageable region of interest (ROI) (Figure 3A). Whether animals moved backward or forward, activity rise of each DD NMJ correlated with ventral relaxation (Figure 3B; Video S3A), and the calcium rise preceded decreased curvature at each ROI (Figures 3A and 3B).

Activation of DD by Chrimson[20] strongly reduced ventral muscle activity (Figure 3C). Unexpectedly, their activation also led to a smaller reduction of dorsal muscle activity (Figure 3C), even though DD motor neurons do not make NMJs to dorsal muscles (Figure 1B).

Inhibition of DD motor neurons by Archaerhodopsin[22] had an opposite effect: a strong increase in ventral muscle activity, and a smaller increase in dorsal muscle activity (Figure 3D; Video S3B). Intriguingly, activity increase of dorsal and ventral muscles exhibited spatial differences: while dorsal activity continued to track curvature, ventral activity became uniform along the

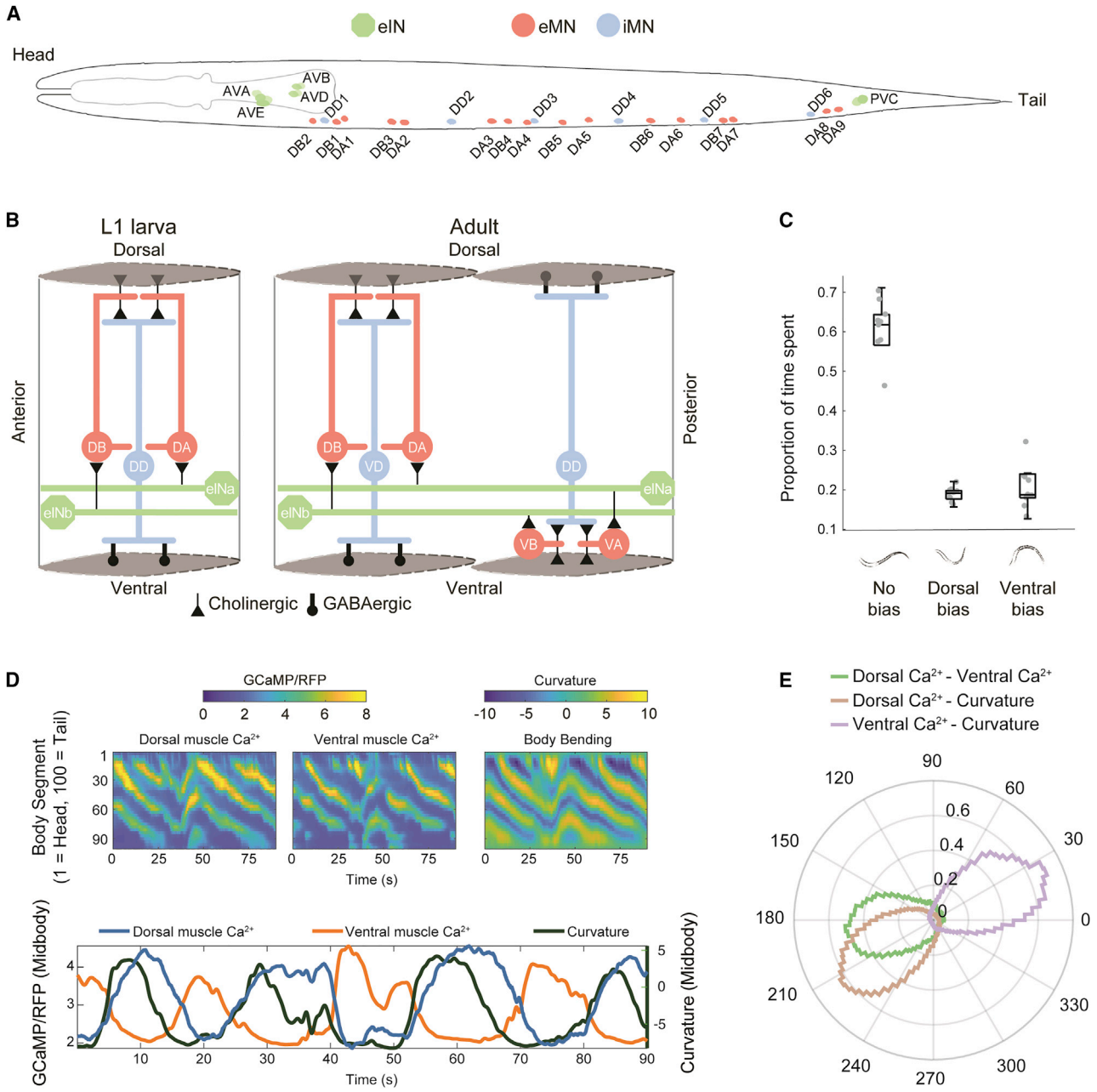

Figure 1. L1 larvae exhibit asymmetry in motor circuit wiring but symmetry in motor pattern

(A) Schematic of the motor circuit for body movement in a newborn L1 larva. Circles denote neuron soma.

(B) Schematic of (left) L1 motor circuit synaptic wiring deduced by our EM reconstruction and (right) adult motor circuit.[3] Diamonds denote muscles. Triangles denote cholinergic synapses. Circles denote GABAergic synapses.

(C) L1 larvae swim without obvious dorsal-ventral bias. n = 10 larvae.

(D) Calcium dynamics of dorsal and ventral muscles in a crawling L1 larva. (Top) Example kymograph of muscle calcium and curvature. (Bottom) Time series of curvature (right y axis) and muscle activity (left y axis) at mid-body.

(E) Polar histograms of phase differences between curvature, dorsal muscle activity, and ventral muscle activity across body (n = 12 larvae).

See also Figure S1, Video S1, and Data S1.

body, decreasing correlation with curvature over time (Figure 3E; Video S3B).

Genetic silencing of DD led to a similar spatial difference. In crawling L1 larvae that do not synthesize GABA (*unc-25*), dorsal muscles exhibited calcium dynamics that correlated with propagating bending waves, whereas calcium signals of ventral muscles did not propagate (Figures 3F and S2; Video S3C).

Therefore, DD motor neurons are inhibitory. These iMNs inhibit ventral muscles with synapses and inhibit dorsal muscles without synapses, implying distinct mechanisms.

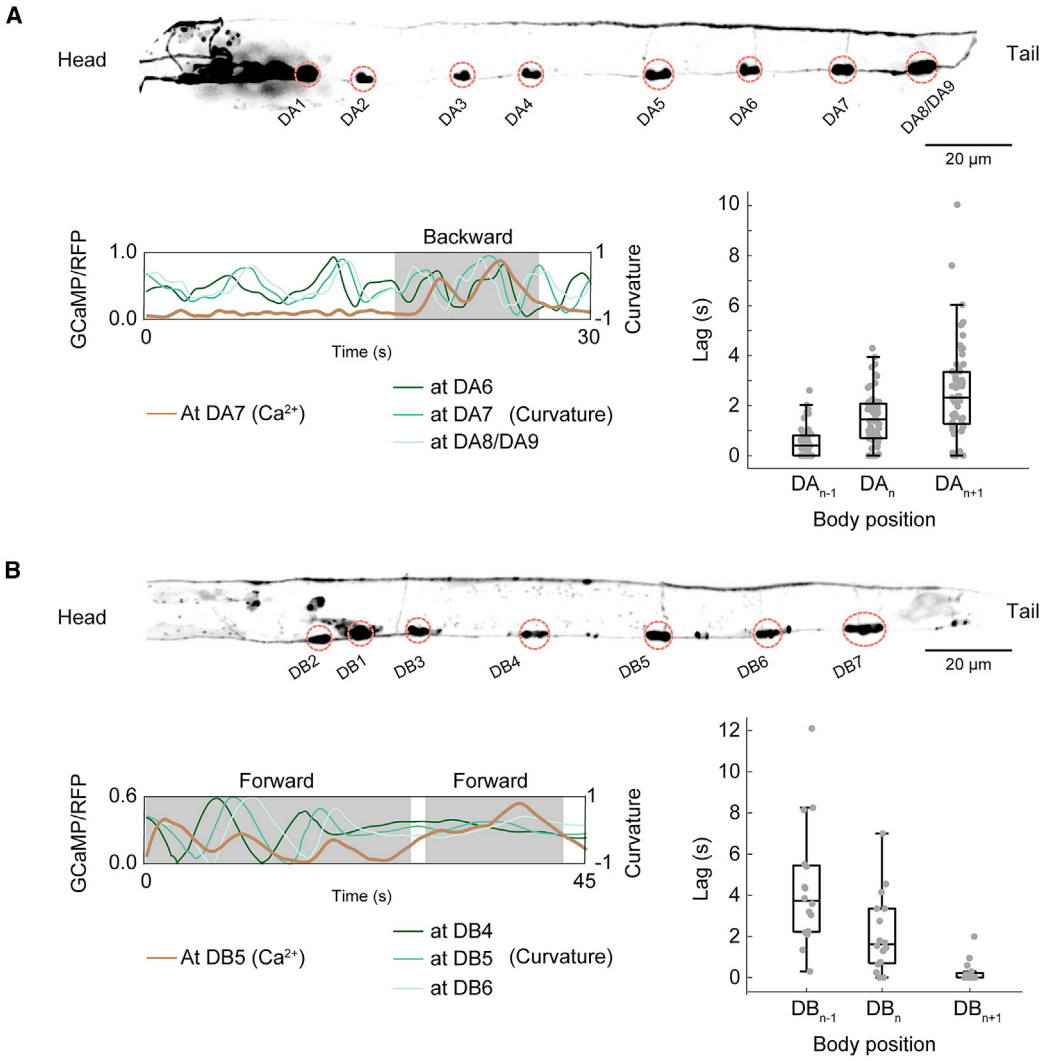

(legend on next page)

Wiring between eMNs and iMNs forms a dorsal bending circuit

Most NMJs from eMNs to dorsal muscles are dyadic synapses, juxtaposing dendrites of iMNs that inhibit the opposing ventral muscles. Thus, activation of dorsal muscles should lead to contralateral ventral muscle inhibition. Consistently, activation of all eMNs by Chrimson[20] increased DD activity (Figure 4A; Videos S4A and S4B). Inhibition of all eMNs by Archaerhodopsin[22] decreased DD activity (Figure 4A; Videos S4C and S4D). Furthermore, ablation of DB eMNs by miniSOG[23] preferentially reduced DD activity when animals attempted forward movement (Figure S3A), whereas ablation of DA reduced DD activity when animals attempted backward movement (Figure S3B).

NMJs to dorsal and ventral muscles drive contraction and relaxation, respectively. Dyadic NMJs from eMNs to iMNs promote relaxation of juxtaposed ventral muscles when dorsal muscles contract. This coordination therefore generates dorsal bending.

Extrasynaptic GABA inhibition plays a dominant role in dorsal muscle relaxation

An exit from dorsal bending requires dorsal muscles to transit from contraction to relaxation. DD motor neurons inhibited both dorsal and ventral muscles but with NMJs to only ventral muscles. This raises the possibility that iMNs inhibit ventral muscle synaptically and dorsal muscles extrasynaptically.

Synaptic and extrasynaptic GABA signals through $GABA_A$ and $GABA_B$ receptors, respectively.[24–26] Consistently, and as reported,[27,28] $GABA_A$ receptors (UNC-49::tagRFP) are present only in ventral muscles (Figure 4C). In their absence (*unc-49* mutants), DD-mediated inhibition of ventral muscles was significantly attenuated whereas inhibition of dorsal muscles was modestly reduced (Figures 4D and 4E). In contrast, in the absence of the functional $GABA_B$ receptor, an obligatory heterodimer[29–31] (*gbb-2* mutants), DD-mediated inhibition of dorsal muscles was significantly attenuated whereas inhibition of ventral muscles was unaffected (Figures 4D and 4E). This indicates a predominant role of extrasynaptic GABA signaling in dorsal muscle relaxation.

Extrasynaptic GABA inhibition of dorsal muscle involves inhibitory feedback of dorsal bending circuit

To address how extrasynaptic GABA inhibits dorsal muscles, we examined where two $GABA_B$ subunits GBB-1 and GBB-2[24–26] reside in L1 larvae.

The dorsal muscle-inhibiting $GABA_B$ subunits are not restricted to dorsal muscles (Figure 4C). GBB-1::GFP signal was weak with most prominent presence in the motor neuron soma. GBB-2::GFP signal was stronger, detectable in motor neuron soma and neurite, dorsal and ventral muscles, and some head neurons. Thus, multiple cells may contribute to dorsal muscle relaxation.

Among them, motor neuron soma, showing prominent overlap of subunit reporters and residing in the closest proximity to GABA, make strong candidates. Indeed, optogenetic activation of DD motor neurons by Chrimson[20] led to strong inhibition of the DA and DB motor neurons, which was attenuated in the absence of $GABA_B$ (*gbb-2* mutants) (Figure 4B). Extrasynaptic GABA signaling may involve negative feedback on eMNs that drive dorsal muscle contraction.

DD inhibition of dorsal muscles was not abolished in *gbb-2* mutant (Figure 4B). Only in larvae without both receptors (*unc-49; gbb-2* mutants) was the inhibition of both dorsal and ventral muscles abolished (Figures 4D and 4E), a response recapitulated by eliminating GABA (*unc-25* mutants) (Figure S4). Despite making a minor contribution to the extent of dorsal muscle inactivation, $GABA_A$ controlled the rate of inhibition in not only ventral but also dorsal muscles (Figure 4F). This supports the negative feedback on the dorsal bending circuit: eMNs are proprioceptive in the adult motor circuit.[8] $GABA_A$-mediated ventral muscle relaxation may further reduce the activity of eMNs.

Therefore, iMNs indirectly relax dorsal muscles through multiple mechanisms. Because of eMN's proximity to GABA, co-expression of $GABA_B$ subunits, and proprioceptive gating, extrasynaptic GABA inhibition to eMNs likely works in concert with the synaptic and extrasynaptic inhibition of ventral muscles to promote the exit from a dorsal bending. The dorsal-bending L1 motor circuit regulates its own exit through negative feedback.

Ventral muscle excitation requires cholinergic premotor interneurons

An exit from dorsal bending, however, is insufficient for ventral bending. The latter requires ventral muscle contraction to occur in synchrony with dorsal muscle relaxation. In the absence of eMN innervation, other mechanisms must excite ventral muscles.

We first considered the simplest possibility:[32,33] a higher myogenic activity of ventral muscles compensates for the absence of motor neuron excitation. However, optogenetic inhibition by GtACR2 of the L1 larva's entire nervous system led to similarly silenced dorsal and ventral muscles (Figure S5A), thus ventral muscle activity is driven by neurons.

We turned to optogenetic stimulation to identify neurons that excite ventral muscles. Because ventral muscles receive inhibitory NMJs, pan-neuronal excitation by Chrimson[20] activated

Figure 2. Cholinergic eMNs underlie dorsal muscle contraction

(A) (Top) GCaMP6s expression in all DA motor neurons. (Bottom) Left shows an example calcium activity trace for DA7 (left y axis) overlaid with curvatures at different body segments (right y axis). Right shows the shortest time lag between DA calcium and curvature anterior (N−1), at (N), and posterior (N+1) to the soma the during backward movement.

(B) The same as in (A) but for DB. Example calcium trace is for DB5. Shortest time lag between DB calcium and curvature changes was calculated during forward movement.

(C) Simultaneous DA and DB activation and muscle calcium imaging. ATR, all-*trans* retinal, opsin-activation co-factor.[19] −ATR (control): 21 epochs (7 larvae); +ATR: 33 epochs (12 larvae).

(D) Simultaneous DA and DB inactivation and muscle calcium imaging. −ATR: 39 epochs (8 larvae); +ATR: 35 epochs (12 larvae). Lines and shades denote median and 95% confidence intervals, respectively.

See also Video S2 and Data S1.

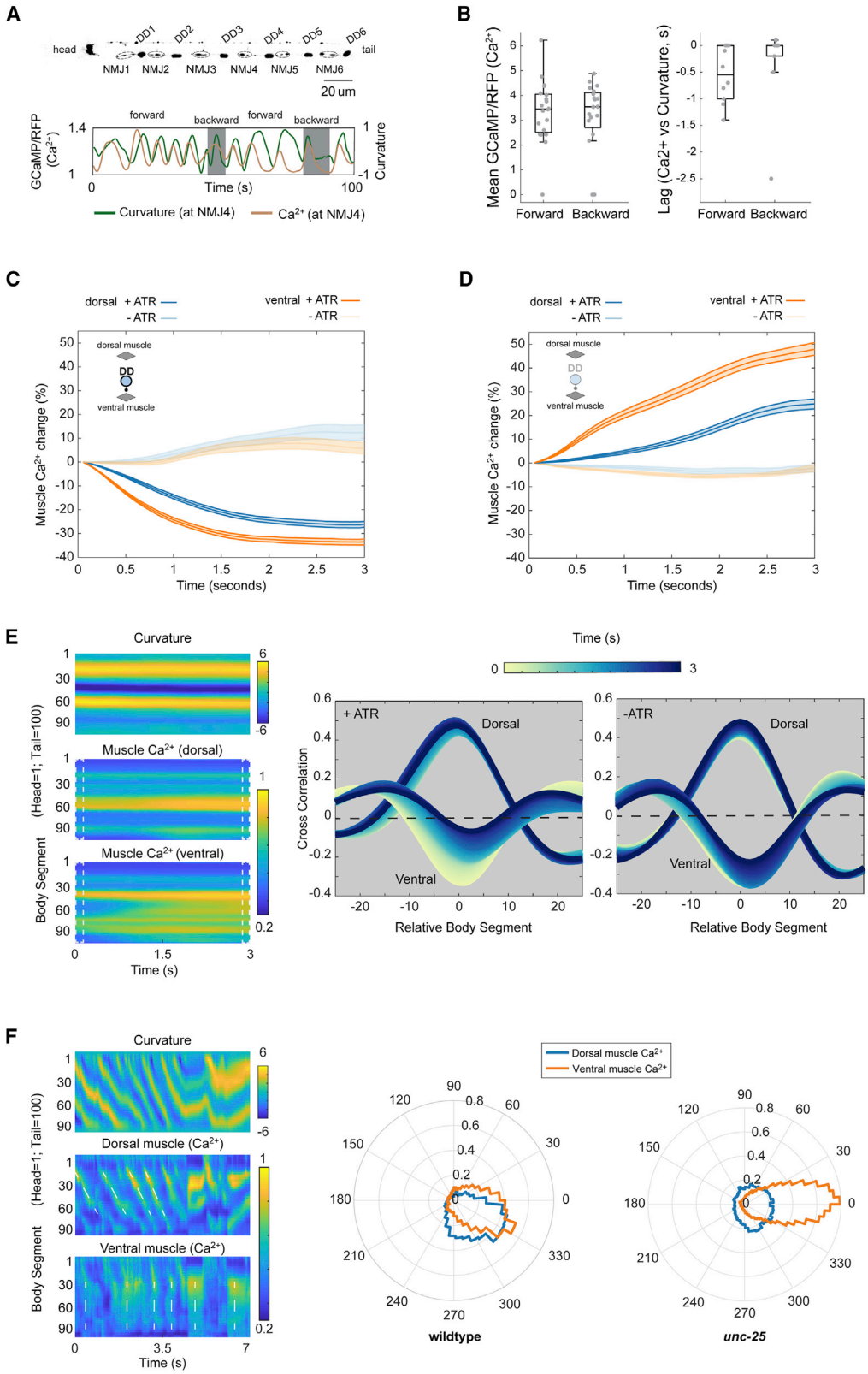

Figure 3. GABAergic iMNs underlie ventral and dorsal muscle relaxation

(A) (Top) GCaMP6s expression in L1 DD, each making a tight cluster of NMJ. NMJn is from DDn. (Bottom) An example calcium trace of NMJ4 (left y axis), overlaid with curvature at the same region (right y axis).

(legend continued on next page)

dorsal muscles but inhibited ventral muscles (Figure S5C). Removing GABA (*unc-25* mutants) revealed activation of dorsal and ventral muscles (Figure S5C). Optogenetic silencing by GtACR2 (Figure S5B) and stimulation by ChR2[19] (Figure S5D) of all cholinergic neurons recapitulated the effects of pan-neuronal manipulation. Thus, cholinergic neurons are responsible for ventral muscle activation.

eINs are cholinergic,[34] and their axons span the ventral nerve cord, making them a candidate source of ventral muscle excitation. Along the nerve cord, two eINs (AVA and PVC) make numerous synapses to all eMNs. eINs also make synapses onto another (Figure 1B). We found that inhibition of eINs by GtACR2 silenced both dorsal and ventral muscles (Figure 5A; Video S5A). In *unc-25* mutants, optogenetic stimulation of eINs by Chrimson[20] activated both dorsal and ventral muscles, with a stronger activation of ventral muscles (Figure 5B; Video S5B). Patterns of dorsal and ventral muscle activity differed, similar to *unc-25* mutants (Figure 3F): dorsal activity was in correlation with curvature, but ventral activity was uniform along the body (Video S5B). These results suggest that ventral muscles are activated by extrasynaptic signaling from cholinergic eINs.

Effects of eIN ablation further support this possibility. In wild-type larvae, eIN-ablation led to diminished ventral muscle activity, with residual dorsal muscle activity (Figure 6A; Videos S6A and S6E). In *unc-25* mutants, ablation of eINs reduced the ventral muscle, but not dorsal muscle activity (Figure 6B; Videos S6B and S6F). Persistent dorsal muscle activity is consistent with endogenous eMN activity in the adult circuit.[7,10]

Premotor interneurons potentiate ventral muscles via extrasynaptic cholinergic signaling

Because eINs do not make synapses to ventral muscles, they may activate ventral muscles either by ephaptic coupling or by extrasynaptic mechanisms that require neurotransmitter release.

We distinguished these two possibilities by assessing the effect of blocking synaptic vesicle fusion using tetanus toxin (TeTx).[35] When vesicular release from all eINs was blocked, activity in both dorsal and ventral muscles was reduced (Figure 6C; Videos S6C and S6G). Reduced dorsal muscle activation is expected, because eINs innervate eMNs. Reduced ventral muscle activation, however, demonstrates that neurotransmitter release is also needed for eINs to activate ventral muscles. Similar to eIN ablation, ventral muscle activity was more severely reduced than dorsal muscles (Figure 6C). Lastly, a reduction of acetylcholine synthesis[36] (*cha-1* RNAi) in all eINs led to more severely reduced ventral muscle activity (Figure S6A).

We propose that cholinergic eINs stimulate ventral muscles through extrasynaptic acetylcholine accumulation, which is consistent with the uniform increase of ventral muscle activity during eIN stimulation.

L1 motor circuit orchestrates dorsal-ventral symmetry by anti-phasic entrainment

With ventral muscles tonically activated, the dorsal-bending motor circuit can entrain ventral muscles to generate complementary ventral bending. An implication of this model is that ventral muscle excitation takes place independently of motor neurons, and dorsal muscle dynamics predict bending.

Consistent with this implication, blocking synaptic transmission from eMNs by TeTx led to higher ventral than dorsal muscle activity (Figure 6D; Video S6D), opposite to the effect of eIN TeTx, a higher dorsal muscle activity (Figure 6C).

Behaviorally, only dorsal muscle calcium signals correlated with a crawling larva's body bending. When eINs or their synaptic output were eliminated, regardless of the level of residual dorsal muscle activity, they led to a persistent bias for dorsal bending, in wild-type and *unc-25* mutant larvae (Figures 6A–6C; Videos S6E-6G). When eMN synaptic output was blocked, regardless of a high ventral muscle activity (Figure 6D), L1 larvae exhibited no consistent dorsal or ventral bending bias across the body (Figure 6D; Video S6H). This coincides with the uniform calcium signal in ventral muscles without correlation with curvature (Figure 6D; Video S6D).

A computational model: Generating a symmetric motor pattern with an asymmetric circuit

We illustrate how bending is generated in each segment (Figure 7A). Dorsal and ventral muscles have similar excitability. Rhythmic dorsal bending is driven by oscillatory activity of cholinergic motor neurons. Cholinergic motor neurons simultaneously activate GABAergic motor neurons that relax ventral muscles. The net effect is a dorsal bend (Figure 7Ai). Rhythmic ventral bending is by anti-phasic entrainment to the oscillator that drives dorsal bends. Ventral muscles are uniformly excited by extrasynaptic acetylcholine from premotor interneurons. This permits ventral bends to passively occur when the dorsal oscillator's activity is low (Figure 7Aiii). Transitions are facilitated by negative feedback within each segment: GABA released by iMNs relaxes ventral muscles and extrasynaptically inhibits eMNs that drive dorsal bending (Figure 7Aii). Thus, in L1 larvae, the same set of motor neurons drive both dorsal and ventral bends. This is in contrast to the adult where two symmetrically wired subcircuits separately underlying dorsal and ventral bends.

We developed a phenomenological model that describes the L1 motor circuit dynamics (Figure 7B). Like the adult,[10] the eMN is modeled as an oscillator (V_{di}) with calcium and potassium

(B) (Left) Mean calcium activity of NMJs during forward and backward movement. N = 17 NMJs (12 larvae); (right) shortest lags between calcium and curvature changes during forward and backward movements.
(C) Simultaneous DD activation and muscle calcium imaging. −ATR (control): 13 epochs (7 larvae); +ATR: 18 epochs (10 larvae).
(D) Simultaneous DD inactivation and muscle calcium imaging in L1 larvae. −ATR (control): 10 epochs (5 larvae); +ATR: 19 epochs (10 larvae). Lines and shades represent median and 95% confidence interval, respectively.
(E) (Left) Example heatmap of curvature, and dorsal and ventral muscle calcium during DD inactivation. (Right) Spatial cross-correlation between the muscle calcium and body curvature during DD inactivation. For ventral muscles, the correlation decreased over time.
(F) (Left) Example heatmap of curvature and muscle calcium signals in a unc-25 larva. (Right) Polar histograms of muscle activity phase lags between segments in wild-type and *unc-25* larvae. n = 10 larvae.
See also Figure S2, Video S3, and Data S1.

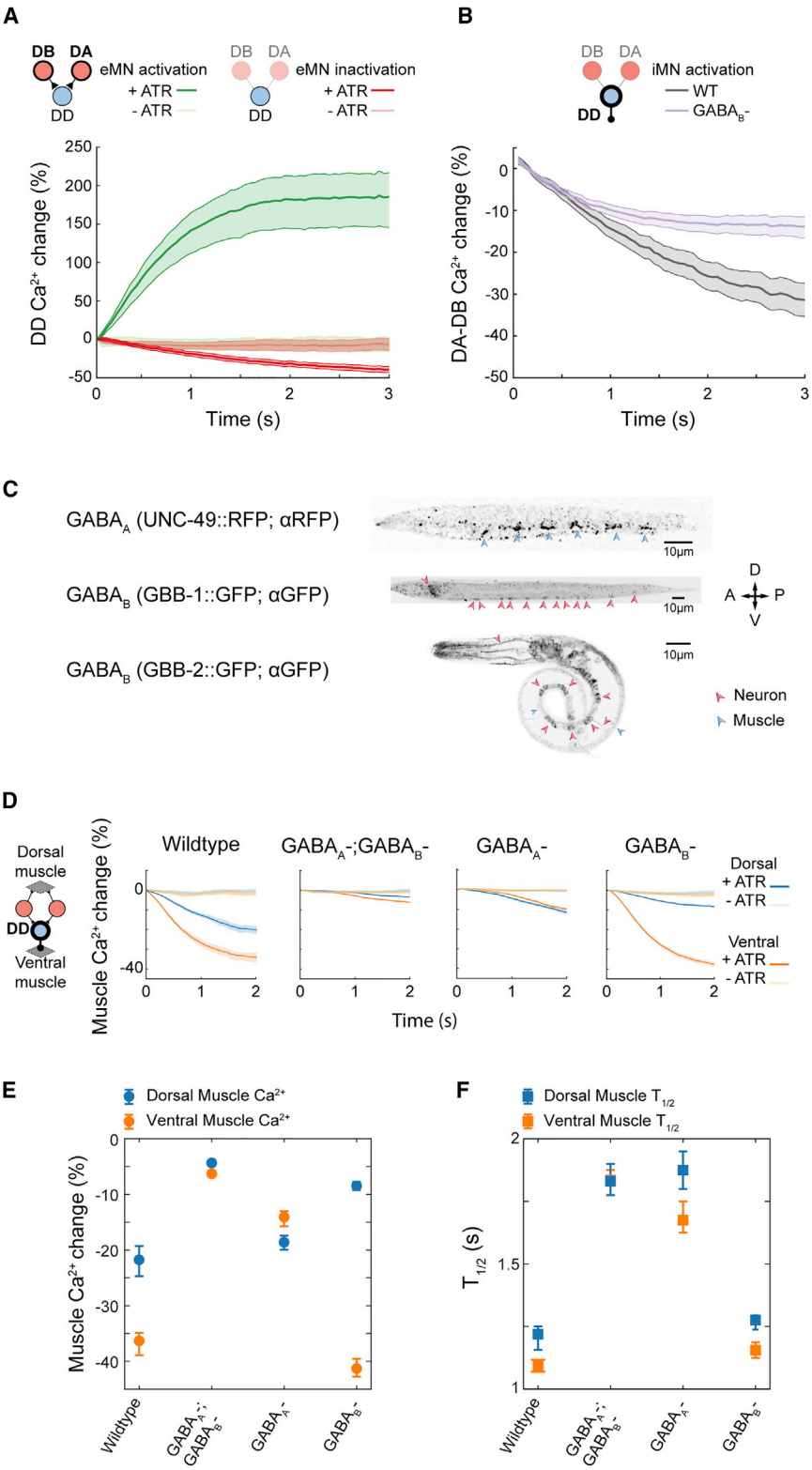

Figure 4. iMNs are activated by eMNs and inhibit muscles by synaptic and extrasynaptic GABA signaling

(A) Optogenetic activation and inactivation of eMNs leads to corresponding changes in iMN activity. (Inset) Schematic depicting the wiring from DA and DB to DD; (green) simultaneous DA and DB activation and DD NMJ calcium imaging. −ATR control: 20 epochs (5 larvae); +ATR: 23 epochs (9 larvae). (Red) Simultaneous DA and DB inaction and DD NMJ calcium imaging. −ATR control: 25 epochs (6 larvae); +ATR: 21 epochs (9 larvae).

(B) Activation of iMN decreases eMN activity, partially dependent on GABAB. (Inset) Schematic depicting the lack of synaptic wiring from DD to DA or DB. Simultaneous DD activation and DA/DB calcium imaging in wild-type and *gbb-2* mutant larvae (+ATR only). Wild-type: 28 epochs (4 larvae); *gbb-2*: 137 epochs (6 larvae).

(C) Expression of endogenously tagged GABAA (UNC-49::RFP) and fosmid reporters for GABAB (GBB-1::GFP and GBB-2::GFP).

(D) Optogenetic activation of iMNs decreases ventral and dorsal muscle activity, with differential requirement of $GABA_A$ and $GABA_B$ receptors. (Inset) Schematic depicting simultaneous iMN activation and muscle calcium imaging. $GABA_A$−; $GABA_B$− mutant: −ATR control: 46 epochs (12 larvae); +ATR: 76 epochs (19 larvae); $GABA_A$ mutants: −ATR control: 37 epochs (22 larvae); +ATR: 51 epochs (20 larvae); $GABA_B$ mutants: −ATR control: 18 epochs (6 larvae); +ATR: 39 epochs (7 larvae).

(E) Maximal activity changes in dorsal and ventral muscles in respective genotypes.

(F) Half-time of dorsal and ventral muscle activity changes in respective genotypes.

Lines and shades in (A), (B), and (D) denote median and 95% confidence intervals.

See also Figures S3 and S4, Video S4, and Data S1.

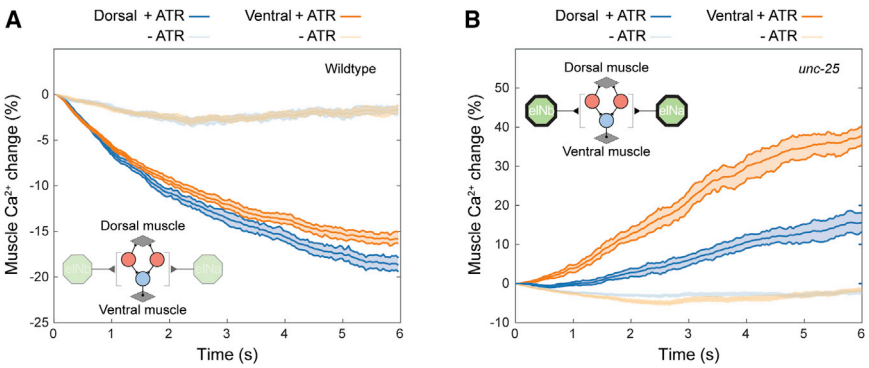

Figure 5. Cholinergic eINs underlie ventral muscle contraction

(A) (Inset) Schematic of simultaneous all eIN inactivation and muscle calcium imaging in wild-type L1 larvae. Inhibition of all eINs reduced both dorsal and ventral muscle activity. −ATR control: 28 epochs (6 larvae); +ATR: 49 epochs (13 larvae). (B) Same as in (A), except for *unc-25* mutants. −ATR control, 51 epochs (17 larvae); +ATR: 43 epochs (12 larvae).

See also Figure S5, Video S5, and Data S1.

conductances. It provides direct input to dorsal muscles (M_{di}) through an excitatory synapse. The eMN relays a copy of input to ventral muscles (M_{vi}), inverting its sign through an inhibitory synapse (*DD*). When dorsal and ventral muscles have the same resting membrane potential, the inhibitory synapse rectifies dorsal oscillations. This produces alternating dorsal-ventral bends with a deeper dorsal bend. An extrasynaptic excitatory input to ventral muscles (*eIN*) alleviates the dorsal bias (Figure 7C).

We modeled propagating bending through proprioceptive input between adjacent eMNs (κ_i). As in previous models,[10,32] directional wave propagation is encoded by curvature-dependent input from $i-1$ (for forward locomotion) or $i+1$ (for backward locomotion). Net bending is calculated from the extent of dorsal and ventral muscle activation in each segment, with parameters obtained by fitting the model outputs to experimental data on dorsal and ventral output symmetry (Figure 6).

Without the inhibitory synapse to ventral muscles, this model predicts a stalled wave on the ventral side. This recapitulates the lack of correlation of ventral muscle activity with bending in *unc-25* mutants (Figure 3F). Perturbation of the inhibitory synapse generates bending with a ventral bias across the body. Behaviorally, *unc-25* mutants exhibited a ventral bias but also generated dorsal bends (Videos S7A and S7B). Our model can recapitulate this phenomenon by adjusting the strength of extrasynaptic input to ventral muscles. This suggests that premotor interneurons may receive feedback from the motor circuit.

Elimination of extrasynaptic input in this model generates dorsal bending across the body, which recapitulates the behavior of eIN-ablated or eIN-vesicle release blocked larvae. Compared to a simpler model, where ventral muscles are spontaneously active, an extrasynaptic excitation confers more flexibility for bending waves.

DISCUSSION

C. elegans is born with only motor neurons that are wired analogously to one motor subcircuit for dorsal bending in adults. Over the course of larval development, neurogenesis and rewiring adds another subcircuit for ventral bending and eliminates asymmetries in the layout of the newborn circuit. However, the larva and adult generate the same undulatory motor pattern. How L1 larvae generate a symmetric motor pattern with an asymmetric circuit has been an enigma. We show that L1 larvae achieve this by using its circuit for dorsal bending to anti-phasically entrain ventral bending, a process that depends on premotor interneurons' tonic potentiation of ventral muscles. Functional compensation by extrasynaptic transmission enables the larva to produce an adult-like undulatory motor pattern before anatomical maturation of the motor circuit.

Result summary

By EM reconstruction and functional imaging and perturbation, we show that in newborn L1 larvae, dorsal muscles receive excitatory NMJs from cholinergic motor neurons whereas ventral muscles receive inhibitory NMJs from GABAergic motor neurons. These inputs are coordinated, thus forming a circuit for dorsal bending. The absence of inhibitory and excitatory synapses to dorsal and ventral muscles respectively raises the possibility of compensation by extrasynaptic signaling. By analyzing GABA receptor mutants, we found that GABAergic motor neurons promote dorsal muscle relaxation, in part through an extrasynaptic feedback inhibition on cholinergic motor neurons that contract dorsal muscles. By optical stimulation, cell ablation, and synapse ablation, we discovered that extrasynaptic cholinergic signaling from premotor interneurons tonically potentiates ventral muscles. Through modeling, we demonstrate that this allows the dorsal bending motor subcircuit to also produce spatially coordinated, anti-phasic ventral bending.

Circuit degeneracy

The *C. elegans* motor circuit offers a profound example of circuit degeneracy where similar functional outputs can have multiple network solutions.[37–39] Other examples include the similar motor patterns exhibited by two molluscs with substantially different functional connectivity[40] and maintenance of a pyloric circuit's output at different temperatures by varying parameters of synaptic connections.[41] Circuit degeneracy has been proposed to play a critical role in population diversity, adaptability to changing environments, and species evolution. Our results demonstrate that degeneracy also minimizes functional disruption to locomotion during development, representing an intrinsic drive to maintain stable motor output in response to ecological demand.

Developmental extrasynaptic signaling

Extrasynaptic signaling is widely observed.[42–46] It is one mechanism for neuromodulation, which allows hard-wired

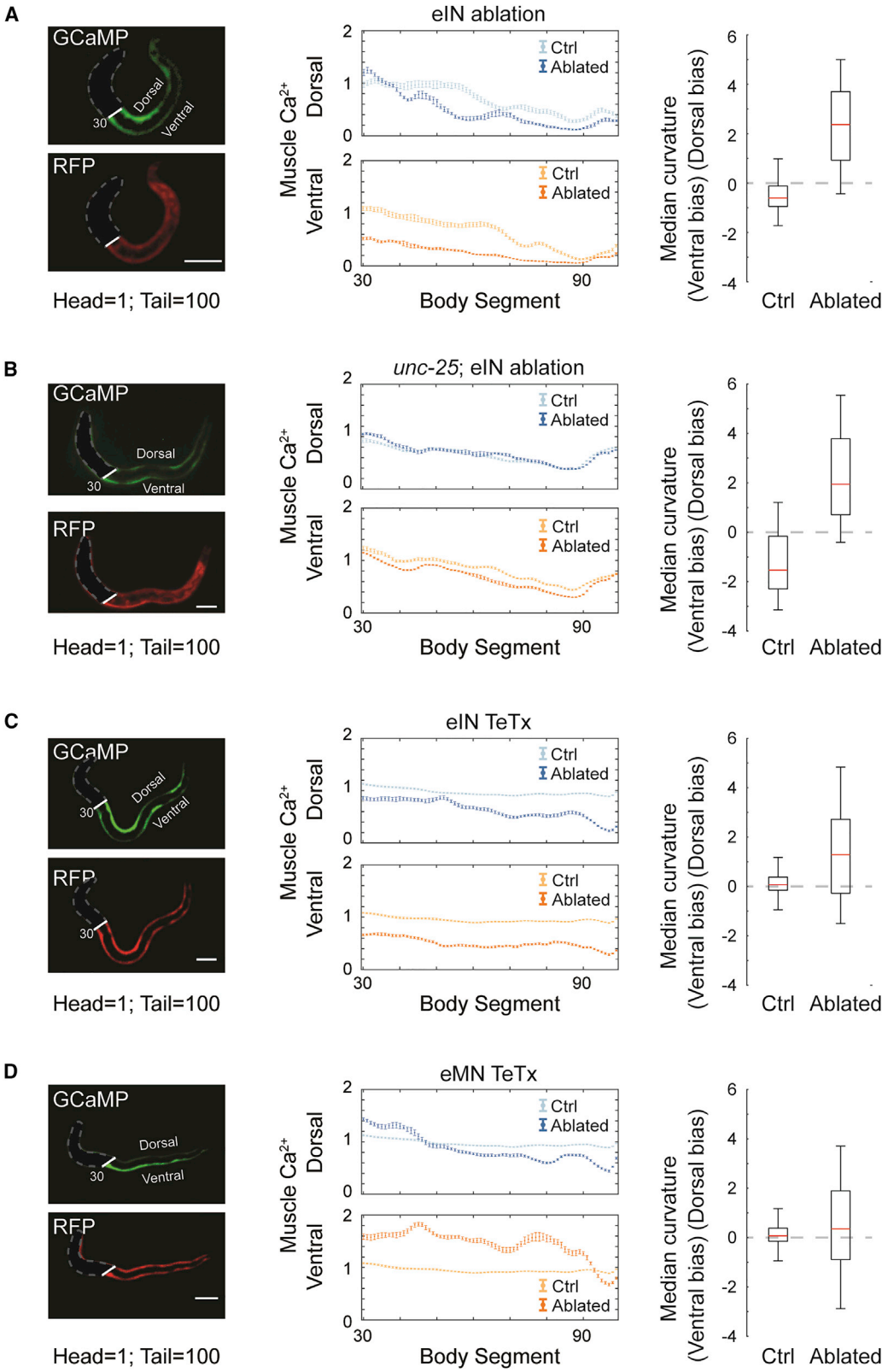

Figure 6. Extrasynaptic transmission from eINs is required for ventral bending

(A–D) Muscle activity and body curvature of L1 larvae that were (A) wild-type with eINs ablated. n = 10 (ctrl) and 11 (ablated) larvae; (B) *unc-25* mutants with eINs ablated. n = 13 (ctrl) and 15 (ablated) larvae; (C) wild-type with eIN vesicle release blocked. n = 10 (ctrl) and 14 (TeTx) larvae; (D) wild-type with eMN vesicle release

(legend continued on next page)

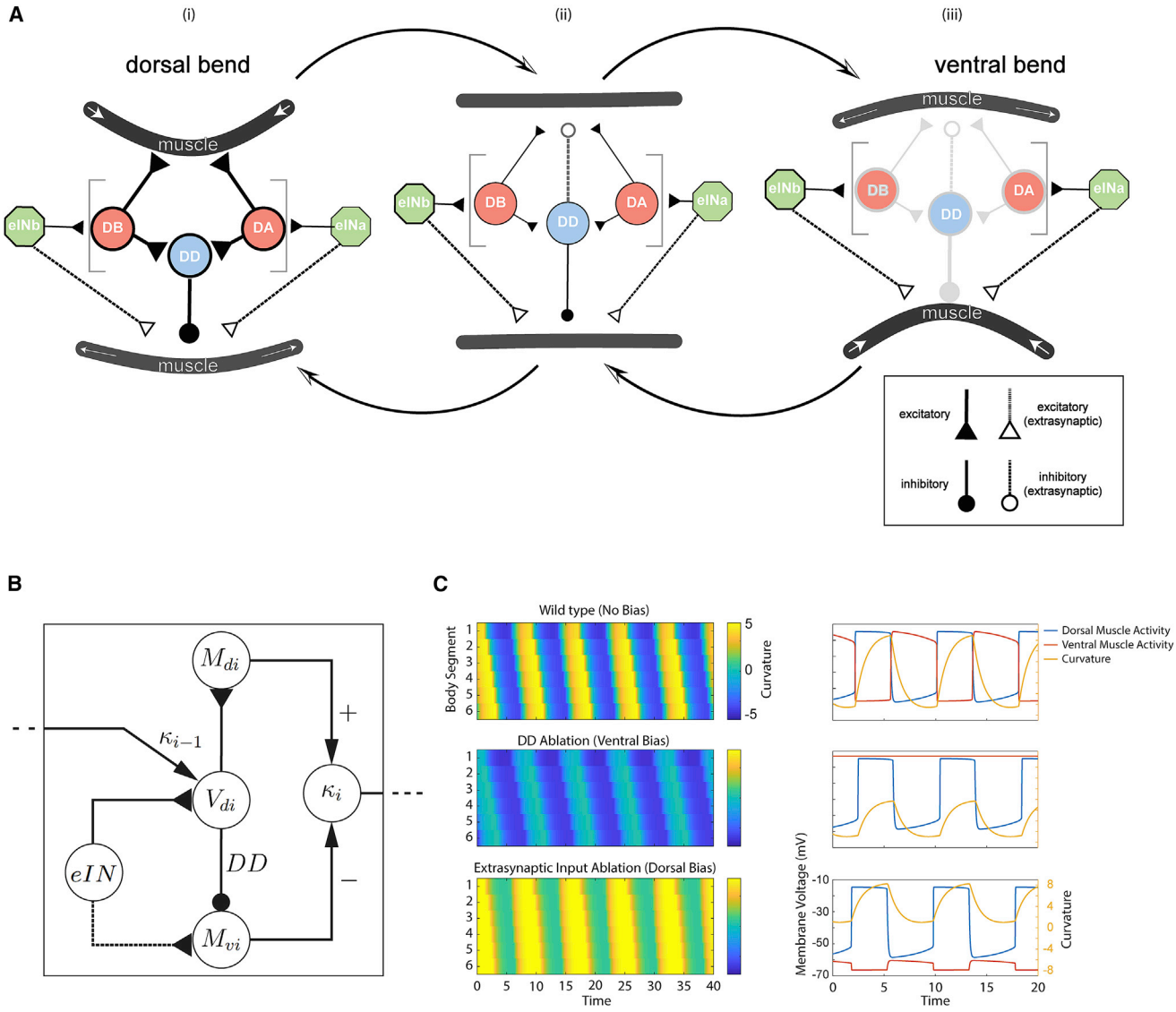

Figure 7. A computational model of the L1 motor circuit

(A) L1 larvae integrate synaptic and extrasynaptic transmission to generate alternating body bends. Schematic depicts transitions (ii) between dorsal bend (i) and ventral bend (iii). White arrows in muscles denote contraction (inward) and relaxation (outward).

(B) Schematic of the computational model at one body segment.

(C) (Left) Curvature kymographs from simulations of the full circuit (top), circuit without inhibitory synapse (middle), and circuit without extrasynaptic excitation (bottom). (Right) Time-series of dorsal and ventral muscle activity and curvature at segment 3.

See also Video S7 and Data S1.

mature circuits to modify and adapt their output to different contexts.[47,48] During *C. elegans* early development, extrasynaptic transmission is essential, compensating for the absence of an entire motor subcircuit. As larvae mature, this role is taken over by post-embryonic motor neurons and synaptic rewiring.[16] Not all extrasynaptic transmission is replaced as the motor circuit matures. Extrasynaptic feedback from GABAergic motor neurons to eMNs persists in the adult.[24–26] It may play similar roles in both dorsal and ventral motor subcircuits. Extrasynaptic mechanisms may work particularly well in L1 larva because of its small size. In a short-lived animal, acquiring full mobility at birth is of probable fitness benefit. Extrasynaptic signaling thus represents an adaptive strategy for development.

blocked. n= 10 (Ctrl); 12 (TeTx) larvae. For (A)–(D): (Left) Example images of muscle GCaMP3::RFP of the experimental group. (Middle) Average dorsal (top) and ventral (bottom) muscle activity in control (lighter lines) and experimental (darker lines) groups. (Right) Median body curvature of experimental and control (Ctrl) groups.

See also Figure S6A, Video S6, and Data S1.

Developmental multi-functionality

In small circuits, individual neurons often adopt multiple functions to expand their behavioral repertoires.[49,50] In the adult, cholinergic motor neurons are rhythm generators for forward and backward movement.[7,9,10] Cholinergic premotor interneurons signal to switch these two modes of locomotion.[10,13] Premotor interneuron calcium imaging (Figure S6B) and activation (Figure S6C) showed that this role is conserved in L1 larvae. However, premotor interneurons assume an additional role in the L1 larva: they directly activate ventral muscles.

The role of premotor interneurons in ventral muscle excitation is likely temporary: the expression of acetylcholinesterase encoding genes, whose enzymatic activity determines extrasynaptic acetylcholine buildup, exhibits a dorsal-ventral asymmetry in the newborn larva.[51] Asymmetry disappears after the L1 stage,[51] coinciding with the emergence of ventral muscle-innervating motor neurons. Therefore, multi-functionality also provides a means to compensate for a circuit's developmental immaturity.

An adequate but temporary solution

In our model, dorsal and ventral muscles are driven by the same oscillators. Consequently, their activation is not fully independent of each other. This implies that synaptic input to dorsal muscles alone determines wave propagation. This prediction recapitulates the experimental outcome of decoupling of dorsal and ventral muscle activity: when we removed synaptic output of dorsal oscillators (eMN-TeTx), or the inhibitory synapse that relays this oscillation to ventral muscles *(unc-25* mutant*),* ventral calcium signals did not propagate and did not correlate with bending.

This configuration differs from the adult, where both dorsal and ventral muscles are driven by dedicated motor subcircuits. Differential activation of dorsal and ventral muscles might have advantages in natural habitats, where *C. elegans* would enable more robust exploration in a 3D environment.[52] Thus, L1 larva's configuration offers an adequate but temporary solution.

STAR★METHODS

Detailed methods are provided in the online version of this paper and include the following:

SUPPLEMENTAL INFORMATION

Supplemental information can be found online at https://doi.org/10.1016/j.cub.2022.09.002.

ACKNOWLEDGMENTS

We thank Ying Wang, Yan Li, Jin Meng, Sway Chen, Yi Li, Bin Yu for technical support; Michael Koelle for discussion; Albert Cardona for CATMAID; and the Human Frontier Science Program Organization RGP0051/2014 (to M.Z. and A.D.T.S.), the Canadian Institutes of Health Research Foundation 154274 (to M.Z.), the National Natural Science Foundation of China (Major International Joint Research Project 32020103007) (to Q.W. and M.Z.), and the National Institute of Health R35 GM134970 and R01 NS093588 (to A.D.C.) for funding.

AUTHOR CONTRIBUTIONS

M.Z. and Q.W. conceived the study; M.Z. supervised the study; Y.L., T.A., A.G., B.M., W.H., J.M., and M.Z. performed experiments and analyzed data; D.W., B.M., D.H., A.C., A.D.C., and M.Z. performed EM; T.A. developed the model; Y.L., T.A., D.W., and Q.W. developed scripts; Y.L., T.A., A.D.T.S., and M.Z. wrote the paper.

DECLARATION OF INTERESTS

The authors declare no competing interests.

Received: December 6, 2021
Revised: June 17, 2022
Accepted: September 1, 2022
Published: September 30, 2022

REFERENCES

1. Croll, N.A. (1975). Components and patterns in the behaviour of the nematode Caenorhabditis elegans. J Zool *176*, 159–176. https://doi.org/10.1111/j.1469-7998.1975.tb03191.x.
2. White, J.G., Albertson, D.G., and Anness, M.A.R. (1978). Connectivity changes in a class of motoneurone during the development of a nematode. Nature *271*, 764–766. https://doi.org/10.1038/271764a0.
3. White, J.G., Southgate, E., Thomson, J.N., and Brenner, S. (1986). The structure of the nervous system of the nematode Caenorhabditis elegans. Philos. Trans. R. Soc. Lond. B Biol. Sci. *314*, 1–340. https://doi.org/10.1098/rstb.1986.0056.
4. Richmond, J.E., and Jorgensen, E.M. (1999). One GABA and two acetylcholine receptors function at the C. elegans neuromuscular junction. Nat. Neurosci. *2*, 791–797. https://doi.org/10.1038/12160.

5. Gao, S., and Zhen, M. (2011). Action potentials drive body wall muscle contractions in Caenorhabditis elegans. Proc. Natl. Acad. Sci. USA *108*, 2557–2562. https://doi.org/10.1073/pnas.1012346108.

6. Liu, P., Ge, Q., Chen, B., Salkoff, L., Kotlikoff, M.I., and Wang, Z.-W. (2011). Genetic dissection of ion currents underlying all-or-none action potentials in C. elegans body-wall muscle cells. J Physiol *589*, 101–117. https://doi.org/10.1113/jphysiol.2010.200683.

7. Gao, S., Guan, S.A., Fouad, A.D., Meng, J., Kawano, T., Huang, Y.-C., Li, Y., Alcaire, S., Hung, W., Lu, Y., Qi, Y.B., Jin, Y., Alkema, M., Fang-Yen, C., and Zhen, M. (2018). Excitatory motor neurons are local oscillators for backward locomotion. Elife *7*, e29915, https://doi.org/10.7554/elife.29915.

8. Wen, Q., Po, M.D., Hulme, E., Chen, S., Liu, X., Kwok, S., Gershow, M., Leifer, A., Butler, V., Fang-Yen, C., Kawano, T., Schafer, W., Whitesides, G., Wyart, M., Chklovskii, D., Zhen, M., and Samuel, A. (2012). Proprioceptive coupling within motor neurons drives C. elegans forward locomotion. Neuron *76*, 750–761. https://doi.org/10.1016/j.neuron.2012.08.039.

9. Fouad, A.D., Teng, S., Mark, J.R., Liu, A., Alvarez-Illera, P., Ji, H., Du, A., Bhirgoo, P.D., Cornblath, E., Guan, S.A., and Fang-Yen, C. (2018). Distributed rhythm generators underlie Caenorhabditis elegans forward locomotion. Elife *7*, e29913, https://doi.org/10.7554/elife.29913.

10. Xu, T., Huo, J., Shao, S., Po, M., Kawano, T., Lu, Y., Wu, M., Zhen, M., and Wen, Q. (2018). Descending pathway facilitates undulatory wave propagation in Caenorhabditis elegans through gap junctions. Proc. Natl. Acad. Sci. USA *115*, E4493–E4502. https://doi.org/10.1073/pnas.1717022115.

11. Wen, Q., Gao, S., and Zhen, M. (2018). Caenorhabditis elegans excitatory ventral cord motor neurons derive rhythm for body undulation. Phil. Trans. Biol. Sci. *373*, 20170370, https://doi.org/10.1098/rstb.2017.0370.

12. Haspel, G., Deng, L., Harreguy, M.B., and Tanvir, Z. (2020). Elegantly. In The Neural Control of Movement (Elsevier), pp. 3–29.

13. Kawano, T., Po, M., Gao, S., Leung, G., Ryu, W., and Zhen, M. (2011). An imbalancing act: gap junctions reduce the backward motor circuit activity to bias C. elegans for forward locomotion. Neuron *72*, 572–586. https://doi.org/10.1016/j.neuron.2011.09.005.

14. Sulston, J.E. (1976). Post-embryonic development in the ventral cord of Caenorhabditis elegans. Philos. Trans. R. Soc. Lond. B Biol. Sci. *275*, 287–297. https://doi.org/10.1098/rstb.1976.0084.

15. Sulston, J.E., and Horvitz, H.R. (1977). Post-embryonic cell lineages of the nematode, Caenorhabditis elegans. Dev. Biol. *56*, 110–156. https://doi.org/10.1016/0012-1606(77)90158-0.

16. Mulcahy, B., Witvliet, D., Mitchell, J., Schalek, R., Berger, D., Wu, Y., Holmyard, D., Lu, Y., Ahamed, T., Samuel, A.D.T., et al. (2022). Post-embryonic maturation of the C. elegans motor circuit. bioRxiv. https://doi.org/10.1101/2022.01.24.477421.

17. Chalfie, M., Sulston, J.E., White, J.G., Southgate, E., Thomson, J.N., and Brenner, S. (1985). The neural circuit for touch sensitivity in Caenorhabditis elegans. J. Neurosci. *5*, 956–964. https://doi.org/10.1523/jneurosci.05-04-00956.1985.

18. Butler, V.J., Branicky, R., Yemini, E., Liewald, J.F., Gottschalk, A., Kerr, R.A., Chklovskii, D.B., and Schafer, W.R. (2015). A consistent muscle activation strategy underlies crawling and swimming in Caenorhabditis elegans. J. R. Soc. Interface *12*, 20140963, https://doi.org/10.1098/rsif.2014.0963.

19. Nagel, G., Brauner, M., Liewald, J.F., Adeishvili, N., Bamberg, E., and Gottschalk, A. (2005). Light activation of channelrhodopsin-2 in excitable cells of Caenorhabditis elegans triggers rapid behavioral responses. Curr. Biol. *15*, 2279–2284. https://doi.org/10.1016/j.cub.2005.11.032.

20. Klapoetke, N.C., Murata, Y., Kim, S.S., Pulver, S.R., Birdsey-Benson, A., Cho, Y.K., Morimoto, T.K., Chuong, A.S., Carpenter, E.J., Tian, Z., Wang, J., Xie, Y., Yan, Z., Zhang, Y., Chow, B.Y., Surek, B., Melkonian, M., Jayaraman, V., Constantine-Paton, M., Wong, G.K.S., and Boyden, E.S. (2014). Independent optical excitation of distinct neural populations. Nat. Methods *11*, 338–346. https://doi.org/10.1038/nmeth.2836.

21. Govorunova, E.G., Sineshchekov, O.A., Janz, R., Liu, X., and Spudich, J.L. (2015). Natural light-gated anion channels: A family of microbial rhodopsins for advanced optogenetics. Science *349*, 647–650. 1979. https://doi.org/10.1126/science.aaa7484.

22. Chow, B.Y., Han, X., Dobry, A.S., Qian, X., Chuong, A.S., Li, M., Henninger, M.A., Belfort, G.M., Lin, Y., Monahan, P.E., and Boyden, E.S. (2010). High-performance genetically targetable optical neural silencing by light-driven proton pumps. Nature *463*, 98–102. https://doi.org/10.1038/nature08652.

23. Qi, Y.B., Garren, E.J., Shu, X., Tsien, R.Y., and Jin, Y. (2012). Photo-inducible cell ablation in Caenorhabditis elegans using the genetically encoded singlet oxygen generating protein miniSOG. Proc. Natl. Acad. Sci. USA *109*, 7499–7504. https://doi.org/10.1073/pnas.1204096109.

24. Schultheis, C., Brauner, M., Liewald, J.F., and Gottschalk, A. (2011). Optogenetic analysis of GABAB receptor signaling in Caenorhabditis elegans motor neurons. J. Neurophysiol. *106*, 817–827. https://doi.org/10.1152/jn.00578.2010.

25. Shen, Y., Wen, Q., Liu, H., Zhong, C., Qin, Y., Harris, G., Kawano, T., Wu, M., Xu, T., Samuel, A.D., and Zhang, Y. (2016). An extrasynaptic GABAergic signal modulates a pattern of forward movement in Caenorhabditis elegans. Elife *5*, e14197, https://doi.org/10.7554/elife.14197.

26. Dittman, J.S., and Kaplan, J.M. (2008). Behavioral impact of neurotransmitter-activated G-protein-coupled receptors: muscarinic and GABAB receptors regulate Caenorhabditis elegans locomotion. J. Neurosci. *28*, 7104–7112. https://doi.org/10.1523/jneurosci.0378-08.2008.

27. Gally, C., and Bessereau, J.-L. (2003). GABA is dispensable for the formation of junctional GABA receptor clusters in Caenorhabditis elegans. J. Neurosci. *23*, 2591–2599. https://doi.org/10.1523/jneurosci.23-07-02591.2003.

28. Pinan-Lucarre, B., Tu, H., Pierron, M., Cruceyra, P.I., Zhan, H., Stigloher, C., Richmond, J.E., and Bessereau, J.-L. (2014). C. elegans Punctin specifies cholinergic versus GABAergic identity of postsynaptic domains. Nature *511*, 466–470. https://doi.org/10.1038/nature13313.

29. White, J.H., Wise, A., Main, M.J., Green, A., Fraser, N.J., Disney, G.H., Barnes, A.A., Emson, P., Foord, S.M., and Marshall, F.H. (1998). Heterodimerization is required for the formation of a functional GABAB receptor. Nature *396*, 679–682. https://doi.org/10.1038/25354.

30. Margeta-Mitrovic, M., Jan, Y.N., and Jan, L.Y. (2000). A trafficking checkpoint controls GABAB receptor heterodimerization. Neuron *27*, 97–106. https://doi.org/10.1016/s0896-6273(00)00012-x.

31. Geng, Y., Bush, M., Mosyak, L., Wang, F., and Fan, Q.R. (2013). Structural mechanism of ligand activation in human GABAB receptor. Nature *504*, 254–259. https://doi.org/10.1038/nature12725.

32. Boyle, J.H., and Cohen, N. (2011). A minimal model of C. elegans forward locomotion: the larval L1 circuit. BMC Neurosci. *12*, P42. https://doi.org/10.1186/1471-2202-12-s1-p42.

33. Gjorgjieva, J., Biron, D., and Haspel, G. (2014). Neurobiology of Caenorhabditis elegans locomotion: where do we stand? Bioscience *64*, 476–486. https://doi.org/10.1093/biosci/biu058.

34. Pereira, L., Kratsios, P., Serrano-Saiz, E., Sheftel, H., Mayo, A.E., Hall, D.H., White, J.G., LeBoeuf, B., Garcia, L.R., Alon, U., and Hobert, O. (2015). A cellular and regulatory map of the cholinergic nervous system of C. elegans. Elife *4*, e12432, https://doi.org/10.7554/elife.12432.

35. Sweeney, S.T., Broadie, K., Keane, J., Niemann, H., and O'Kane, C.J. (1995). Targeted expression of tetanus toxin light chain in Drosophila specifically eliminates synaptic transmission and causes behavioral defects. Neuron *14*, 341–351. https://doi.org/10.1016/0896-6273(95)90290-2.

36. Rand, J.B. (1989). Genetic analysis of the cha-1-unc-17 gene complex in Caenorhabditis. Genetics *122*, 73–80. https://doi.org/10.1093/genetics/122.1.73.

37. Marder, E., Goeritz, M.L., and Otopalik, A.G. (2015). Robust circuit rhythms in small circuits arise from variable circuit components and

mechanisms. Curr. Opin. Neurobiol. *31*, 156–163. https://doi.org/10.1016/j.conb.2014.10.012.

38. Powell, D.J., Marder, E., and Nusbaum, M.P. (2021). Perturbation-specific responses by two neural circuits generating similar activity patterns. Curr. Biol. *31*, 4831–4838.e4. https://doi.org/10.1016/j.cub.2021.08.042.
39. Calabrese, R.L. (2021). Neuronal networks: Degeneracy unleashed. Curr. Biol. *31*, R1439–R1441. https://doi.org/10.1016/j.cub.2021.09.023.
40. Sakurai, A., and Katz, P.S. (2017). Artificial synaptic rewiring demonstrates that distinct neural circuit configurations underlie homologous behaviors. Curr. Biol. *27*, 1721–1734.e3. https://doi.org/10.1016/j.cub.2017.05.016.
41. O'Leary, T., and Marder, E. (2016). Temperature-robust neural function from activity-dependent ion channel regulation. Curr. Biol. *26*, 2935–2941. https://doi.org/10.1016/j.cub.2016.08.061.
42. Trueta, C., and De-Miguel, F.F. (2012). Extrasynaptic exocytosis and its mechanisms: a source of molecules mediating volume transmission in the nervous system. Front. Physiol. *3*, 319. https://doi.org/10.3389/fphys.2012.00319.
43. Jobson, M.A., Valdez, C.M., Gardner, J., Garcia, L.R., Jorgensen, E.M., and Beg, A.A. (2015). Spillover transmission is mediated by the excitatory GABA receptor LGC-35 in C. elegans. J. Neurosci. *35*, 2803–2816. https://doi.org/10.1523/jneurosci.4557-14.2015.
44. De-Miguel, F.F., and Fuxe, K. (2012). Extrasynaptic neurotransmission as a way of modulating neuronal functions. Front. Physiol. *3*, 16. https://doi.org/10.3389/fphys.2012.00016.
45. Zoli, M., Torri, C., Ferrari, R., Jansson, A., Zini, I., Fuxe, K., and Agnati, L.F. (1998). The emergence of the volume transmission concept. Brain Res. Rev. *26*, 136–147. https://doi.org/10.1016/s0165-0173(97)00048-9.
46. Vizi, E.S., Fekete, A., Karoly, R., and Mike, A. (2010). Non-synaptic receptors and transporters involved in brain functions and targets of drug treatment. Br. J. Pharmacol. *160*, 785–809. https://doi.org/10.1111/j.1476-5381.2009.00624.x.
47. Marder, E. (2012). Neuromodulation of neuronal circuits: back to the future. Neuron *76*, 1–11. https://doi.org/10.1016/j.neuron.2012.09.010.
48. Bentley, B., Branicky, R., Barnes, C.L., Chew, Y.L., Yemini, E., Bullmore, E.T., Vértes, P.E., and Schafer, W.R. (2016). The multilayer connectome of Caenorhabditis elegans. PLoS Comput. Biol. *12*, e1005283, https://doi.org/10.1371/journal.pcbi.1005283.
49. Getting, P.A. (1989). Emerging principles governing the operation of neural networks. Annu. Rev. Neurosci. *12*, 185–204. https://doi.org/10.1146/annurev.ne.12.030189.001153.
50. Briggman, K.L., and Kristan, W.B., Jr. (2008). Multifunctional pattern-generating circuits. Annu. Rev. Neurosci. *31*, 271–294. https://doi.org/10.1146/annurev.neuro.31.060407.125552.
51. Combes, D., Fedon, Y., Toutant, J.-P., and Arpagaus, M. (2003). Multiple ace genes encoding acetylcholinesterases of Caenorhabditis elegans have distinct tissue expression. Eur. J. Neurosci. *18*, 497–512. https://doi.org/10.1046/j.1460-9568.2003.02749.x.
52. Bilbao, A., Patel, A.K., Rahman, M., Vanapalli, S.A., and Blawzdziewicz, J. (2018). Roll maneuvers are essential for active reorientation of Caenorhabditis elegans in 3D media. Proc. Natl. Acad. Sci. USA *115*, E3616–E3625. https://doi.org/10.1073/pnas.1706754115.
53. Mulcahy, B., Witvliet, D., Holmyard, D., Mitchell, J., Chisholm, A.D., Meirovitch, Y., Samuel, A.D.T., and Zhen, M. (2018). A pipeline for volume electron microscopy of the Caenorhabditis elegans nervous system. Front Neural Circuits *12*, 94. https://doi.org/10.3389/fncir.2018.00094.
54. Witvliet, D., Mulcahy, B., Mitchell, J.K., Meirovitch, Y., Berger, D.R., Wu, Y., Liu, Y., Koh, W.X., Parvathala, R., Holmyard, D., Schalek, R.L., Shavit, N., Chisholm, A.D., Lichtman, J.W., Samuel, A.D.T., and Zhen, M. (2021). Connectomes across development reveal principles of brain maturation. Nature *596*, 257–261. https://doi.org/10.1038/s41586-021-03778-8.
55. Cardona, A., Saalfeld, S., Schindelin, J., Arganda-Carreras, I., Preibisch, S., Longair, M., Tomancak, P., Hartenstein, V., and Douglas, R.J. (2012). TrakEM2 software for neural circuit reconstruction. PLoS One *7*, e38011, https://doi.org/10.1371/journal.pone.0038011.
56. Schindelin, J., Arganda-Carreras, I., Frise, E., Kaynig, V., Longair, M., Pietzsch, T., Preibisch, S., Rueden, C., Saalfeld, S., Schmid, B., Tinevez, J.Y., White, D.J., Hartenstein, V., Eliceiri, K., Tomancak, P., and Cardona, A. (2012). Fiji: an open-source platform for biological-image analysis. Nat. Methods *9*, 676–682. https://doi.org/10.1038/nmeth.2019.
57. Saalfeld, S., Cardona, A., Hartenstein, V., and Tomančák, P. (2009). CATMAID: collaborative annotation toolkit for massive amounts of image data. Bioinformatics *25*, 1984–1986. https://doi.org/10.1093/bioinformatics/btp266.
58. Liao, E.H., Hung, W., Abrams, B., and Zhen, M. (2004). An SCF-like ubiquitin ligase complex that controls presynaptic differentiation. Nature *430*, 345–350. https://doi.org/10.1038/nature02647.
59. Lim, M.A., Chitturi, J., Laskova, V., Meng, J., Findeis, D., Wiekenberg, A., Mulcahy, B., Luo, L., Li, Y., Lu, Y., Hung, W., Qu, Y., Ho, C.Y., Holmyard, D., Ji, N., McWhirter, R., Samuel, A.D., Miller, D.M., Schnabel, R., Calarco, J.A., and Zhen, M. (2016). Neuroendocrine modulation sustains the C. elegans forward motor state. Elife *5*, e19887, https://doi.org/10.7554/elife.19887.
60. Guo, Z. v, Hart, A.C., and Ramanathan, S. (2009). Optical interrogation of neural circuits in Caenorhabditis elegans. Nat. Methods *6*, 891–896. https://doi.org/10.1038/nmeth.1397.
61. Rickgauer, J.P., Deisseroth, K., and Tank, D.W. (2014). Simultaneous cellular-resolution optical perturbation and imaging of place cell firing fields. Nat. Neurosci. *17*, 1816–1824. https://doi.org/10.1038/nn.3866.
62. Akerboom, J., Carreras Calderón, N., Tian, L., Wabnig, S., Prigge, M., Tolö, J., Gordus, A., Orger, M.B., Severi, K.E., Macklin, J.J., Patel, R., Pulver, S.R., Wardill, T.J., Fischer, E., Schuler, C., Chen, T.W., Sarkisyan, K.S., Marvin, J.S., Bargmann, C.I., Kim, D.S., Kugler, S., Lagnado, L., Hegemann, P., Gottschalk, A., Schreiter, E.R., and Looger, L.L. (2013). Genetically encoded calcium indicators for multi-color neural activity imaging and combination with optogenetics. Front. Mol. Neurosci. *6*, 2. https://doi.org/10.3389/fnmol.2013.00002.
63. Kim, C.K., Yang, S.J., Pichamoorthy, N., Young, N.P., Kauvar, I., Jennings, J.H., Lerner, T.N., Berndt, A., Lee, S.Y., Ramakrishnan, C., Davidson, T.J., Inoue, M., Bito, H., and Deisseroth, K. (2016). Simultaneous fast measurement of circuit dynamics at multiple sites across the mammalian brain. Nat. Methods *13*, 325–328. https://doi.org/10.1038/nmeth.3770.
64. Packer, A.M., Russell, L.E., Dalgleish, H.W.P., and Häusser, M. (2015). Simultaneous all-optical manipulation and recording of neural circuit activity with cellular resolution in vivo. Nat. Methods *12*, 140–146. https://doi.org/10.1038/nmeth.3217.
65. Rajasethupathy, P., Sankaran, S., Marshel, J.H., Kim, C.K., Ferenczi, E., Lee, S.Y., Berndt, A., Ramakrishnan, C., Jaffe, A., Lo, M., Liston, C., and Deisseroth, K. (2015). Projections from neocortex mediate top-down control of memory retrieval. Nature *526*, 653–659. https://doi.org/10.1038/nature15389.
66. Zhang, Z., Russell, L.E., Packer, A.M., Gauld, O.M., and Häusser, M. (2018). Closed-loop all-optical interrogation of neural circuits in vivo. Nat. Methods *15*, 1037–1040. https://doi.org/10.1038/s41592-018-0183-z.
67. Morris, C., and Lecar, H. (1981). Voltage oscillations in the barnacle giant muscle fiber. Biophys. J. *35*, 193–213. https://doi.org/10.1016/s0006-3495(81)84782-0.
68. Wicks, S.R., Roehrig, C.J., and Rankin, C.H. (1996). A dynamic network simulation of the nematode tap withdrawal circuit: predictions concerning synaptic function using behavioral criteria. J. Neurosci. *16*, 4017–4031. https://doi.org/10.1523/jneurosci.16-12-04017.1996.

STAR★METHODS

KEY RESOURCES TABLE

REAGENT or RESOURCE	SOURCE	IDENTIFIER
Antibodies		
RFP antibody [5F8]	Chromotek	Cat#5f8; RRID: AB_2336064
GFP monoclonal antibody [3E6]	Invitrogen	Cat#A-11120; RRID:AB_221568
Bacterial strains		
E. coli	*Caenorhabditis* Genetics Center	RRID: WB-STRAIN:OP50-1
Experimental models		
C. elegans	This paper	Data S1
Recombinant DNA		
Plasmids and fosmids	This paper	Data S1
Software and algorithms		
ImageJ	NIH Image	RRID: SCR_003070
NIS elements	Nikon	RRID: SCR_014329
MATLAB	MathWorks	RRID: SCR_001622
GraphPad Prism	GraphPad	RRID: SCR_002798
Codes		
Github	This paper	https://github.com/zhen-lab/Beta_Function_Analysis
Nomenclature and reagent guides		
Nomenclature and reagents	This paper	Data S1

RESOURCE AVAILABILITY

Lead contact

Further information and requests for resources and reagents should be directed to and will be fulfilled by the lead contact, Mei Zhen (meizhen@lunenfeld.ca).

Materials availability

Constructs and strains generated in this study are available from the lead contact upon request.

Data and code availability

- All original code has been deposited at GitHub and is publicly available. A link to the repository is listed in the key resources table.
- Any additional information required to reanalyze the data reported in this paper is available from the lead contact upon request.

EXPERIMENTAL MODEL AND SUBJECT DETAILS

C. elegans strains were grown and maintained on nematode growth media (NGM) plates seeded with the *Escherichia coli* strain OP50 at 20-22.5°C. All constructs and strains used in this study are listed in key resources table and Data S1.

METHOD DETAILS

Construction of transgenic strains

Transgenic ZM strains were generated by injecting fosmid or plasmid constructs (pJH) at 2-50ng/μl, with respective injection markers into indicated genetic backgrounds, to produce those with extra chromosomal arrays (*hpEx*). They were integrated into the genome by UV irradiation of *hpEx* lines followed by selective screening and outcrossing against N2 wild-type strains (*hpIs*). Other transgenic arrays or strains were acquired from either *CGC* or individual laboratories. A reagent guide, which provides detailed information and usage of constructs and strains are listed in Data S1, in supplemental information.

Synchronization of young L1 larvae for all behavioral and imaging experiment

L1 larvae used for behavioral and imaging experiments were collected as follows. On the day of experiment, up to one hundred 3-fold stage eggs from plates with well-fed gravid adults were transferred to a new plate seeded with OP50. Eggs were allowed to hatch for 1hr at 22.5°C and unhatched eggs were removed. Most experiments were carried out 5-6 hours afterwards to ensure that they had not integrated post-embryonically derived motor neurons.[14] Some transgenic lines grew a bit slower, so experiments were carried out 8-10hr afterwards.

Electron microscopy of an early L1 stage larva

Serial electron microscopy was performed as previously described (Figures 1B and S1).[53,54] The L1 larva reconstructed here was at an early L1 stage (~1-5hr), prior to the beginning of post-embryonic neurogenesis that starts at 6hr. It covers over half of the body, and was manually serial sectioned at 50nm thickness and imaged by TEM at 0.7nm/pixel. Images were stitched into 3D volumes using TrakEM2 Fiji plugin,[55,56] and annotated after skeleton tracing in the CATMAID.[57] A full reconstruction of the ventral and dorsal nerve cords of a newborn L1 larva (1hr) revealed the same pattern and is described in another study.[16]

Imaging of GABA receptors on L1 larvae

GABA receptors were visualized by either direct imaging of tagged fluorescent proteins or immunostaining (Figure 3C). For $GABA_A$ receptor UNC-49, UNC-49 is tagged with RFP and visualized for RFP fluorescence. The larvae were fixed with 2% paraformaldehyde and 25% methanol to mitigate autofluorescence. Immunostaining of L1 larvae for GBB-1::GFP and GBB-2::GFP with anti-GFP antibodies after fixation was carried out as described.[58]

Analyses of swimming animals

Light field recording of swimming wildtype L1 larvae was performed in a PDMS miniature well (Figure 1C). A droplet of M9 was mounted onto the center of the well or chamber, and L1 larvae were individually transferred into the droplet. With a coverslip mounted, the PDMS well was placed on a glass slide and recorded with a 4x objective with a customized compound microscope[13] for 68s at 26Hz. After images were acquired, body postures were manually scored frame-by-frame. Ventral side of the larva was identified by the presence of anus and/or the gonad. A dorsal-biased bending posture was defined by a convex towards the dorsal side from the neck (30%) to the tail. A ventral-biased bending posture was defined by a convex towards the ventral side from the neck (30%) to the tail. Other postures include both dorsal and ventral bending and were deemed 'unbiased'. Frames where neither the anus nor the gonad could be confidently identified were discarded. The total number of frames each larva spent in one of three postures was normalized against the total number of frames for each recording.

Behavioral imaging of swimming L1 larvae

Example movies for swimming wild type and *unc-25* L1 larvae were recorded in a chamber made with a thin circle of Vaseline between two glass slides (Videos S1A and S7B). The chamber was filled with S-basal culture media and multiple L1 larvae. Recordings were carried out with a 10X objective of a Zeiss dissecting microscope (V16) and a Basler aca2500-60μm CCD camera with the Pylon viewer program, for 2-5min at 10Hz.

Calcium imaging of muscle and curvature analyses of crawling animals

L1 Larvae expressing GCaMP3 and tagRFP separately in body wall muscles were used in these experiments (Figures 1D, 1E, and 3F; Videos S1C and S3C). Dual-color recording of GCaMP3 and mCherry was performed using an in-house ImageJ plugin as described.[13,59] L1 larvae were mounted with a small droplet of M9 or halocarbon oil. Recordings were performed with 20x or 40x objectives, at 26Hz, 20Hz or 10Hz, for 68s, 90s or 180s, respectively, typically by manual stage tracking to keep moving animals in the center of view. Analysis of these images to extract muscle calcium signals are detailed in the "quantification and statistical analysis" section below.

Calcium imaging of neurons and curvature analyses in crawling animals

L1 Larvae expressing GCaMP::RFP fusion in neurons were used in these experiments (Figures 2A, 2B, 3A, and 3B; Figures S6B and S6C; Videos S2 and S3A). Recordings were acquired on a customized LED-powered wide-field tracking compound microscope with L1 larvae slowly crawling on 2% agarose pads under a coverslip. Dual-color recording of GCaMP6 and mCherry was performed using an in-house ImageJ plugin as described.[13,59] L1 larvae were mounted with either a small droplet of M9 or halocarbon oil. Recordings were performed with 40x or 63x objectives, at 26Hz, 20Hz or 10Hz, for 68s, 90s or 180s, typically by manual stage tracking. Analysis of calcium imaging is described in the "quantification and statistical analysis" section below.

A simple strategy for simultaneous optogenetic stimulation and calcium imaging

Simultaneous functional imaging and optogenetic stimulation is technically challenging due to the overlapping excitation spectra for opsins and genetic calcium sensors. Two strategies to address this issue are to spatially separate the illumination[60,61] or to attempt spectral separation of opsins and calcium sensors.[61–66]

We approached simultaneous optogenetic stimulation and calcium imaging with a simpler goal. Because calcium readout exhibits significant latency compared to the light response of opsin channels, and opsins can be activated by the same illumination spectra for

GCaMP and RFP, the initial change of calcium signals should already reflect the cell's response to opsin stimulation. We validated this strategy with a characterized connection (cholinergic motor neurons to their downstream GABAergic motor neurons in adults), and then applied it to examine the complete L1 motor circuit.

The following protocol conducts bi-directional (activation and inhibition) functional manipulation with any combination between all tested opsins (ChR2, Chrimson, GtACR2) and calcium sensors (GCaMP::RFP and chameleon). It can be carried out on wide-field fluorescent as well as confocal microscopes. The following protocol is not meant to probe dynamics of circuit connectivity. It is a simple but effective assay to establish causality and functional connectivity between neurons.

We used the same wide-field fluorescent microscope for calcium imaging (Figures 2C, 2D, 3C–3E, 4A, 4B, and 4D–4F; Figures S4 and S5; Videos S3B, S4, and S5). Strains that express opsins in upstream cells and calcium sensors in downstream cells were cultured on all-trans retinal (ATR)-supplemented plates for multiple generations. A control group was cultured on plates without ATR. For experimental groups, particularly strains generated from the Cre-LoxP system, animals were cultured on plates supplied with higher concentration ATR (250μM) to increase the strength of optogenetic stimulation. On the day of experiments, L1 larvae were mounted on slides as described for neuron calcium imaging, except that they were immobilized by limited M9 solution. One minute after samples were mounted, recording was carried out initially without the LED light. During the recording, the LED light (serving both for calcium imaging and opsin stimulation) was turned on and off, with an on phase longer than 3 seconds (3s), and off phase ranging from 5-20s. Sampling rates ranged from 10-26Hz. Calcium imaging analyses were carried out as described above. A maximum of 5 randomly selected epochs from each animal were included to prevent biased representation, and only the first 3-6s recording for each epoch was used for analyses.

Calcium imaging and curvature analyses upon eIN and eMN manipulation

Calcium imaging of freely crawling animals. Calcium imaging recordings for Figure 6 were performed with unconstrained L1 larvae, hatched on a thin lawn of OP50 of 2% agarose plates with S-basal buffer. Images were acquired with a Nikon T1 (model Ti2-E) spinning disk confocal microscope operating in a widefield mode with a 10x objective at 10fps. The setup was equipped with a dual view system and Andor Zyla VSC-07720 camera (Videos S6A and S6B). Toptica's multi-laser system was used for illumination at 10mW power. Imaging analyses was carried out using a MATLAB script as described below.

Photo-ablation of neurons by miniSOG. Transgenic animals that express blue light activated miniSOG protein were used in these experiments, performed, and verified as described (Figures 6A and 6*;* Figure S3*;* Videos S6A and S6B).[7] Briefly, to visually examine ablation efficiency, miniSOG was co-expressed with SL2-RFP to tag the to-be-ablated neurons and neurites. Cells that activated apoptosis usually appear vacuolar after the light treatment. But the complete disappearance of soma and neurites could only be observed towards the end of the larval stage. A home-made chamber delivers the blue LED light, dissipates heat, and supplies oxygen by ventilation during illumination. For each experiment, eggs were picked onto the OP50 lawn of an imaging plate. After hatching for 1hr, all unhatched eggs were removed. The plate with 1hr post-hatching larvae were then placed in the chamber upright with its lid removed. The optimal exposure time was experimentally determined for each strain to ablate cells without arresting larva growth. The eIN-ablation strain required 30min exposure, and the eMN-ablation strain required 15 minute exposure. After illumination, animals were allowed to recover in darkness for 4hr before behavioral and calcium imaging experiments. The control group larvae were similarly hatched on OP50 seeded plates and maintained alongside the experimental group (larvae plates) after their LED treatment. The larger variation in these control groups (compared to the Control groups in Figures 6C and 6D, which were wildtype animals) was likely caused by their exposure to blue and red laser during calcium imaging experiments. It takes up to two days for ablated neurons to anatomically disintegrate and absorbed by other tissues. To verify successful ablation of neurons, after each larva was imaged, it was recovered and transferred to individual NGM culture plates with OP50 to grow for two days into adulthood. They were then examined for RFP signals using a compound microscope. Only data recorded from those with absence of RFP in targeted neurons were used for analyses.

Wide-field imaging and analyses of crawling animals

On plate recording of free crawling L1s. Recordings were performed using a customized wide-field, white-light compound microscope,[13] one larva at a time, with a thin-layer of OP50 bacteria food on a NGM plate (Videos S1B, S6E–S6H, and S7A). Larva movements manually tracked to stay in the center of view during recording, typically for 75s at 26Hz.

On plate recording free crawling L1s upon optogenetic stimulation): For each set of optogenetic experiments, the control and experimental group contained animals of the same genotype, with the control group cultured on plates without ATR (Figures S6B and S6C). All larvae were recorded using image plates that were unseeded with OP50 and without ATR, typically for 75s at 26Hz. Animals in the experimental group was cultured on NGM plates supplied with 0.1mg/ml ATR for at least two generations. Individual L1 larvae were transferred to and recorded using the same unseeded imaging plate as described above. L1 larvae from the control group were recorded on a separate imaging plate. All animals were subjected to stimulation from an LED light source controlled by a customized ImageJ plugin.[13] The stimulation protocol was 10s light-off (pre-stimulation), 4 consecutive epochs of stimulation consisting of 10s light-on and 5s light-off, followed by 10s light-off (post-stimulation).

A computational model

We modeled each segment of the L1 motor circuit using the equations below (1-5), which is schematized in Figure 7B. The model is inspired by the Morris-Lecar model of the Barnacle giant muscle fiber.[67] It's a reduced order nonlinear model with an instantaneous

calcium current, a potassium current with an activation variable, and a passive leak current. A similar model was used previously to study adult *C. elegans* excitatory motor neurons.[10] We model 6 segments coupled to each other proprioceptively, corresponding to the 6 DD NMJs. V_{di}, M_{di}, M_{vi} are the membrane potentials for the eMN, dorsal muscle and ventral muscle in segment i, respectively. n_i is the activation variable for the slow potassium current and κ_i is the segment's curvature. We implicitly model the activity of DD iMNs via an inhibitory synapse on ventral muscles by eMNs. We did not include the extrasynaptic inhibition to dorsal muscles in our model, because it was not necessary for the generation of a symmetric oscillatory gait. This also recapitulates our experimental findings, where inhibitory feedback on to dorsal muscles is modulatory and *gbb-1* mutant larvae do not exhibit overt motor defects.

$$C_m\frac{dV_{di}}{dt} = -g_L(V_{di}-E_L) - g_{Ca}m_\infty(V_{di})(V_{di}-E_{Ca}) - g_K n_{di}(V_{di}-E_K) + c\kappa_{i-1} + I_{SYN+}^{V_{eIN}} \quad (1)$$

$$\tau_n\frac{dn_{di}}{dt} = -n_{di} + n_\infty(V_{di}) \quad (2)$$

$$\tau_u\frac{dM_{di}}{dt} = -M_{di} + I_{SYN+}^{V_{di}} \quad (3)$$

$$\tau_u\frac{dM_{vi}}{dt} = -M_{vi} + I_{SYN-}^{V_{di}} + I_{SYN\star}^{V_{eIN}} \quad (4)$$

$$\tau_b\frac{d\kappa_i}{dt} = -\kappa_i + \sigma(M_{di}) - \sigma(M_{vi}) \quad (5)$$

Where $E_L = -60\,mV, E_{Ca} = 60\,mV, E_K = -70\,mV$ are the leak, calcium, and potassium reversal potentials, respectively. Terms $g_L = 100\,pS, g_{Ca} = 400\,pS, g_K = 500\,pS$ are the maximal leak, calcium, and potassium conductances and $C_m = 3\,pF$ is the membrane capacitance. Timescale parameters were set as $\tau_n = 30\,ms, \tau_u = 85\,ms, \tau_b = 10\,ms$.

The function $m_\infty(V) = \frac{1}{1+\exp\left(\frac{V_m - V}{\theta_m}\right)}$ with $\theta_m = 10.25\,mV, V_m = -29\,mV$ and $n_\infty(V) = \frac{1}{1+\exp\left(\frac{V_n - V}{\theta_n}\right)}$ with $\theta_n = 20\,mV, V_n = -55\,mV$, while $\sigma(V) = \alpha(\tanh(\beta * V) + 1)$ with $\alpha = 1000\,mm^{-1}$ and $\beta = 0.01\,mV^{-1}$ converts muscle activities to curvature.

The terms $I_{SYN+}^{V_{di}}, I_{SYN+}^{V_{eIN}}, I_{SYN-}^{V_{di}}, I_{SYN\star}^{V_{eIN}}$ are the synaptic currents from the excitatory synapse from to dorsal muscles, excitatory synapse from eINs to eMNs, inhibitory synapse from eMNs to ventral muscles, and the excitatory extrasynaptic input from eINs to ventral muscles, respectively. The synaptic currents are based on the graded synapse model,[68] and are defined as follows.

$$I_{SYN+}^{V_{di}} = g(V_{di})(M_{di} - E^+)$$

$$I_{SYN+}^{V_{eIN}} = g(V_{eIN})(V_{di} - E^+)$$

$$I_{SYN-}^{V_{di}} = g(V_{di})(M_{vi} - E^-)$$

$$I_{SYN\star}^{V_{eIN}} = g(V_{eIN})(M_{vi} - E^\star)$$

$$g(V) = \frac{\bar{g}}{1+\exp\left\{K\left(\frac{V_k - V}{V_{range}}\right)\right\}}$$

With $K = 2\ln\left(\frac{0.1}{0.9}\right)$, set such that the conductance varied from 10% to 90% of its maximum value over the presynaptic voltage range set by V_{range}. Other parameters were set as $\bar{g} = 1\,nS, V_k = -30\,mV, V_{range} = 20\,mV$. Terms $E^+, E^-, E^\star$ are the reversal potentials for the excitatory receptor, the inhibitory receptor and the extrasynaptic receptor. We set $E^+ = -10\,mV$. E^- *and* $E^\star$ were treated as variables and optimized to result in an unbiased gait, such that the mean value of the bending curvature κ_i is zero. The optimized values were found to be $E^- = -67\,mV, E^\star = 33.5\,mV$.

QUANTIFICATION AND STATISTICAL ANALYSIS

Analysis of muscle calcium data

Post-imaging analyses used customized MATLAB scripts. The head and tail are manually assigned in the first frame of the recording and tracked afterwards. The contour of the worm is extracted from images. Its mid-line was divided into 100 segments (0 for the head and 100 for the tail), along the anterior-posterior axis, and further segmented into the dorsal and ventral sub-segments across the mid-line. Averaged fluorescent intensity within each segment is used as proxy for the activity for this muscle segment. Bending curvatures were derived from the derivatives of the tangent angles at each segment (Figures 1D, 1E, and 3F; Videos S1C and S3C).

Analysis of neuronal calcium and curvature

Calcium imaging analyses were carried out using a MATLAB script modified from a previous study[8] that tracks individual regions of interest (ROI) (Figures 2A, 2B, 3A, 3B, S6B, and S6C; Videos S2 and S3A). Intensity of individual ROI in the green and red channels was used to calculate calcium dynamics. Curvature at individual ROI was estimated by angles between its immediate neighbours.

Calculation of phase differences between calcium signals and bending

Phase differences between dorsal muscle activity, ventral muscle activity, and curvature were carried out using the Hilbert transform, through the MATLAB's Hilbert function (Figures 1E and 3F, and S2). Time-series were converted to a complex number representation, which was then used to estimate the phase angles at each time-point. Distribution of the differences between phase angles from all samples was then plotted as polar histograms.

Velocity measurements of crawling animals

Velocity calculation was carried out using customized MATLAB scripts (Figure S6B and S6C). Briefly, contours of recorded L1 larva images above were segmented and divided into 100 segments along the anterior-posterior axis. Orientation (head, tail, ventral, and dorsal) were manually assigned in the first frame of the recording and tracked automatically. Errors were fixed by manual curation afterwards. Instantaneous velocity was measured by the displacement of centroid between frames; those towards the head are forward movement and those towards the tail are backward movement.

Statistical analysis

Standard boxplots showing minimum, 25^{th} percentile, median, 75^{th} percentile, and maximum of the data excluding outliers are used (Figures 2A, 2B, 3B, and 6). All error bars reported are computed as 95% confidence intervals of the reported statistic by bootstrapping over 1000 samples randomly sampled with replacement (Figures 2C, 2D, 3C, 3D, 4A, 4B, 4D, 4E, 4F, 5, 6, S4, S5, and S6A). p values reported are computed by the Wilcoxon matched-pairs signed rank test (Figures S6B and S6C).

Current Biology, Volume *32*

Supplemental Information

Extrasynaptic signaling enables an asymmetric juvenile motor circuit to produce symmetric undulation

Yangning Lu, Tosif Ahamed, Ben Mulcahy, Jun Meng, Daniel Witvliet, Sihui Asuka Guan, Douglas Holmyard, Wesley Hung, Quan Wen, Andrew D. Chisholm, Aravinthan D.T. Samuel, and Mei Zhen

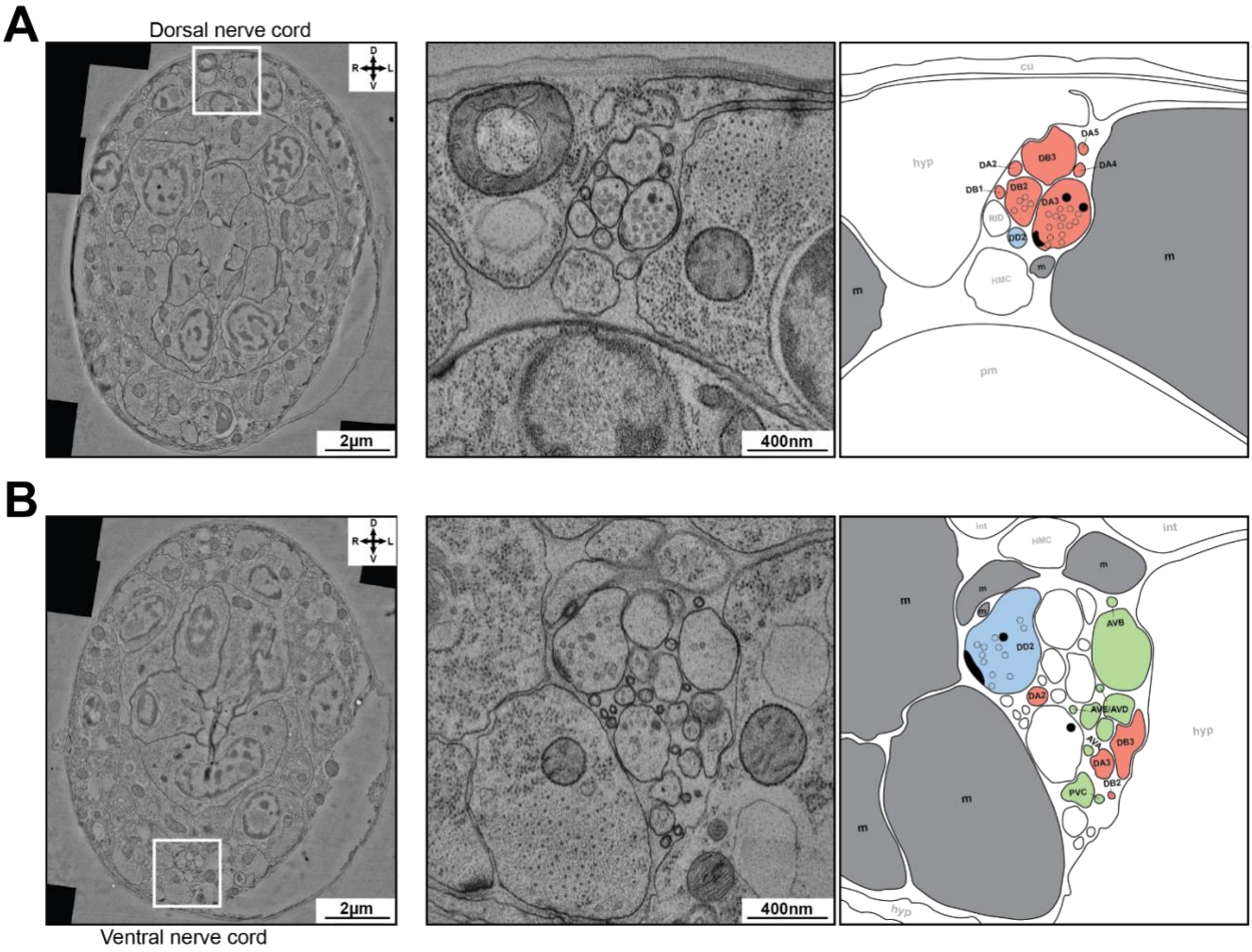

Figure S1. Electron microscopy reconstruction of the dorsal and ventral nerve cord of a 5-6hr L1 larva, related to Figure 1.

(A) Example image of the dorsal nerve cord. (Left) An electron micrograph of the cross-section in transverse plane. The dorsal nerve cord is marked. (Middle) An enlarged view of the dorsal nerve cord. (Right) Cross-sections of individual neurites of motor neurons and muscles of the L1 motor circuit were color-coded and annotated. Red: eMNs; blue: iMNs; grey: muscles. One eMN (DA3) makes a dyadic NMJ to the muscle and iMN (DD2), with an active zone (black crescent), a cluster of synaptic vesicles (clear circles), and sparse dense core vesicles (dark circles).

(B) Example image of the ventral nerve cord, similarly illustrated and annotated as in (A). Neurites for eINs, which are absent from the dorsal nerve cord (A), are color-coded green. An iMN (DD2) makes a NMJ to muscles. In right panels, cross-sections of other neuron (RID) and cell (HMC) of the L1 motor circuit in the dorsal nerve cord (A) and ventral nerve cord (B) were labelled by opaque letters. Abbreviations: m: muscle; pm: pharyngeal muscle; hyp: hypodermis; cu: cuticle; int: intestine.

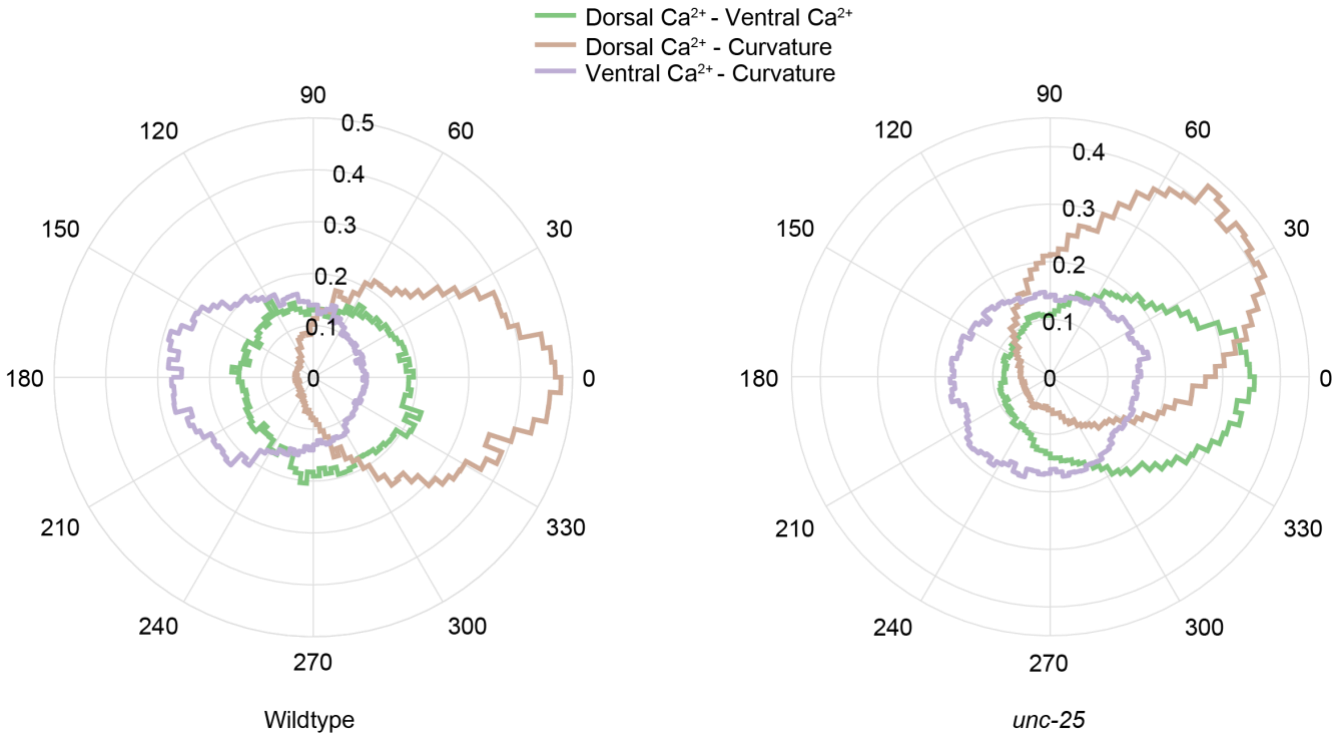

Figure S2. Calcium dynamics of dorsal muscles tracks bend waves in *unc-25* mutant larvae, related to Figure 3.

Polar histograms of the phase differences between curvature, dorsal muscle activity, and ventral muscle activity (segments 33-95) for crawling wildtype and *unc-25* larvae imaged under the same condition. (Left) In wildtype larvae, dorsal muscle activity was in phase with body bending and ventral muscle was anti-phasic with body bending. (Right) In *unc-25* larvae, ventral muscles had no phase relationship with curvature, but dorsal muscle activity tracked body bending with phase lag. N = 10 recordings for each group.

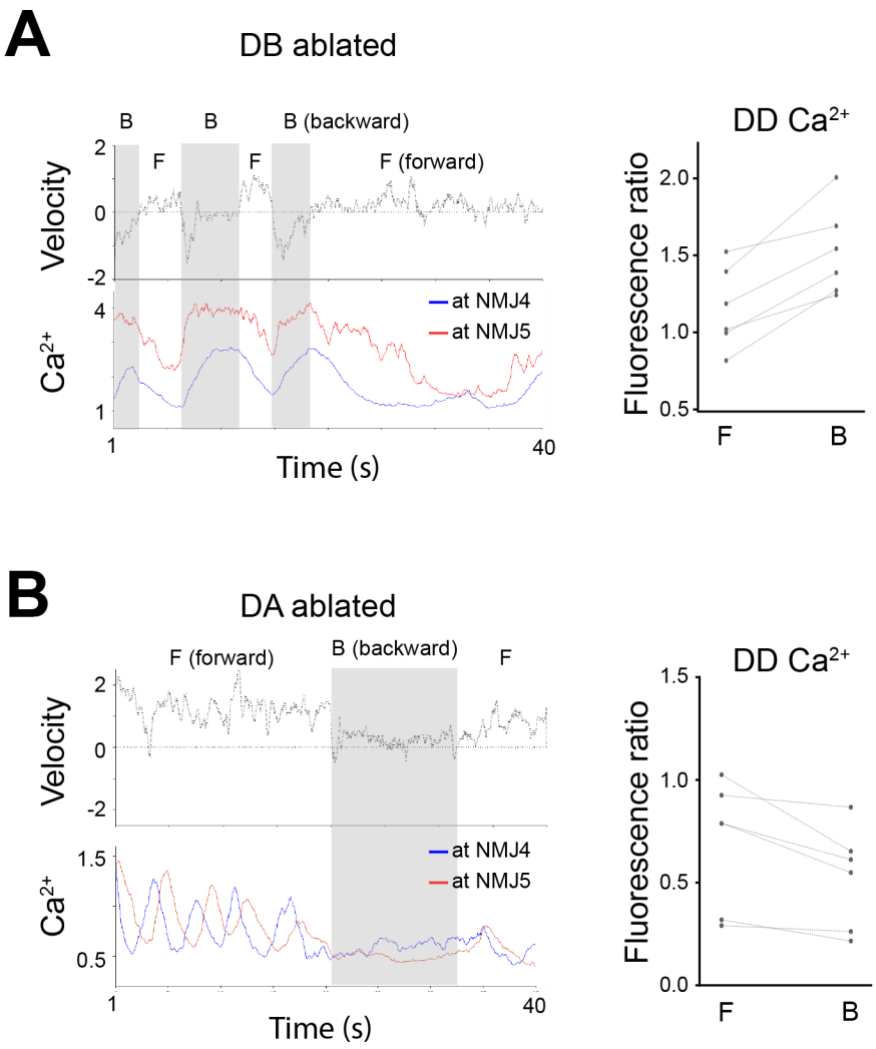

Figure S3. Ablation of eMNs reduces iMN activity during directional movement, related to Figure 4.

(A) (Left) Example of velocity and DD NMJ calcium of an L1 lava upon DA ablation. It still transited between forward and backward movement, with fictive reversals shown as pauses. (Right) Mean DD activity during forward and backward movement. lines connect epochs from the same animals.

(B) (Left) Example of velocity and DD NMJ calcium of an L1 lava upon DB ablation. It still transited between forward and backward movement, with fictive forward shown as pauses. (Right) Mean DD activity during forward and backward movement. Lines connect epochs from the same animals.

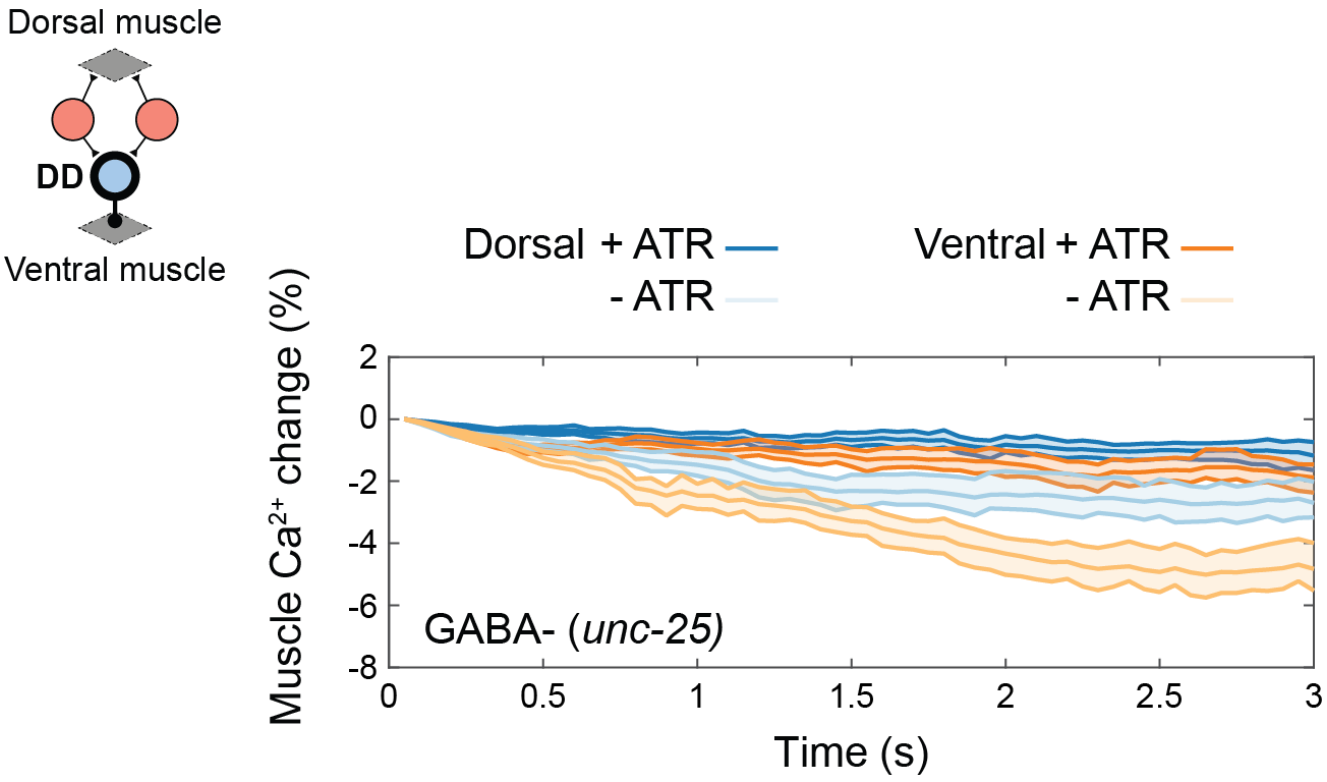

Figure S4. Activation of iMNs does not significantly reduce ventral and dorsal muscle activity in mutant larvae that do not synthesize GABA, related to Figure 4.

(Inset) Schematic of simultaneous optogenetic activation of iMNs and muscle calcium imaging. Y-axis plots percentage changes of the muscle activity from t = 0. ATR: *all trans retinal,* a cofactor for opsion activation. Control group (-ATR): 34 stimulation epochs from 12 larvae; Experimental group (+ATR): 15 stimulation epochs from 5 larvae.

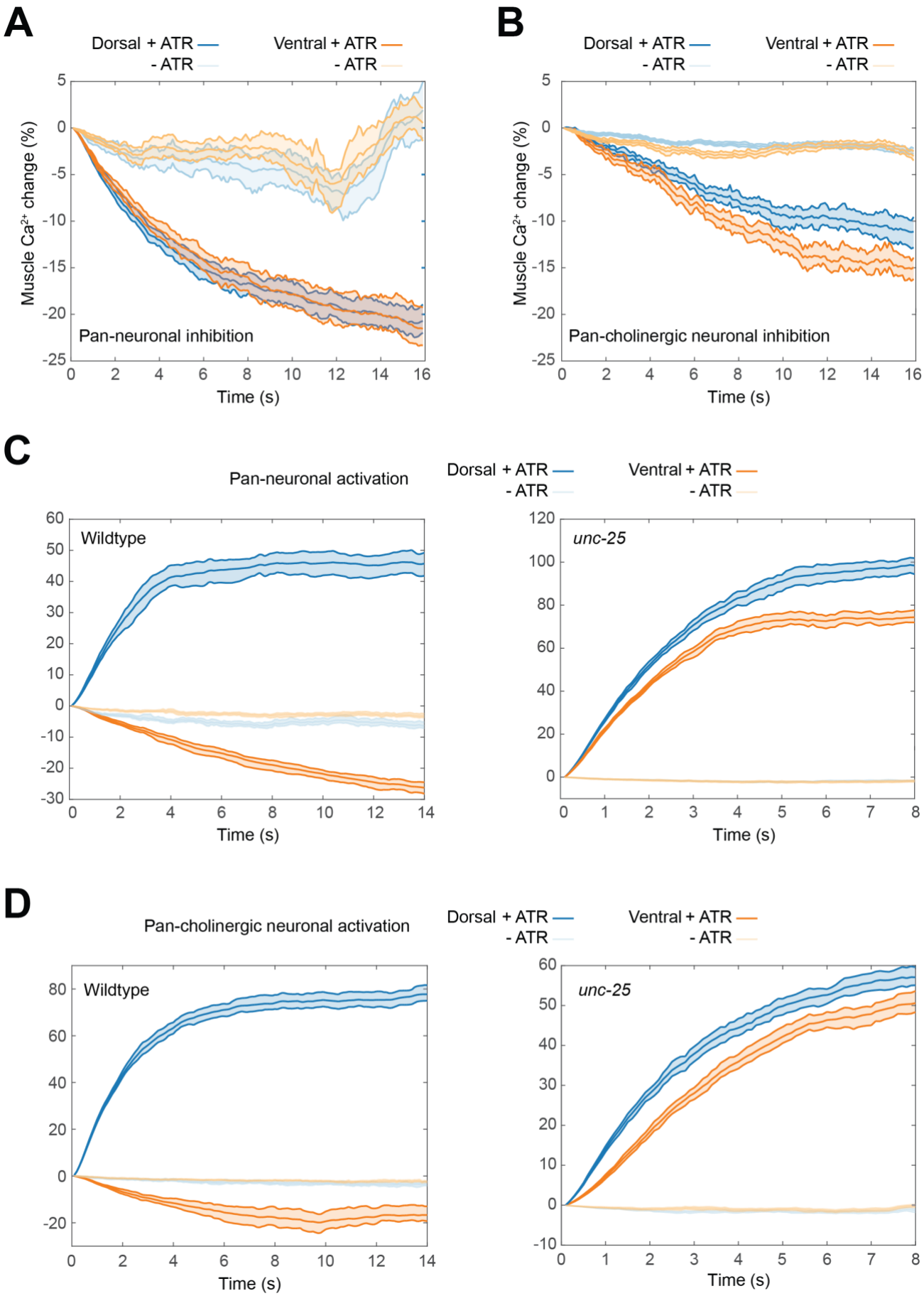
A
Dorsal + ATR
- ATR
Ventral + ATR
- ATR
Muscle Ca2+ change (%)
Pan-neuronal inhibition
Time (s)
B
Dorsal + ATR
- ATR
Ventral + ATR
- ATR
Muscle Ca2+ change (%)
Pan-cholinergic neuronal inhibition
Time (s)
C
Pan-neuronal activation
Dorsal + ATR
- ATR
Ventral + ATR
- ATR
Wildtype
unc-25
Time (s)
D
Pan-cholinergic neuronal activation
Dorsal + ATR
- ATR
Ventral + ATR
- ATR
Wildtype
unc-25
Time (s)

Figure S5. Effect of optogenetic manipulation of groups of neurons on dorsal and ventral muscles, related to Figure 5.

(A-B) Muscle calcium responses upon optogenetic silencing of all neurons (A) or all cholinergic neurons (B) in wildtype larvae. Y-axis plots percentage changes of the muscle activity. Panneuronal inhibition: the control group (-ATR): 18 epochs from 6 larvae; the experimental group (+ATR): 26 epochs from 12 larvae. Cholinergic neuron inhibition: the control group (-ATR), 16 epochs from 3 larvae; the experimental group (+ATR), 27 epochs from 5 larvae.

(C) Muscle calcium responses upon optogenetic activation of all neurons in wildtype (left) or *unc-25* mutant (right) larvae. Wildtype group: -ATR: 17 epochs from 9 larvae; +ATR: 18 epochs from 10 larvae. *unc-25* group: -ATR: 14 epochs from 9 larvae; +ATR: 21 epochs from 11 larvae.

(D) Muscle calcium responses upon activation of all cholinergic neurons in wildtype (left) or *unc-25* mutant (right) larvae. Wildtype group: -ATR, 15 epochs from 7 larvae; +ATR, 19 epochs from 10 larvae. *unc-25* group: -ATR, 18 epochs from 6 larvae; +ATR, 30 epochs from 10 larvae.

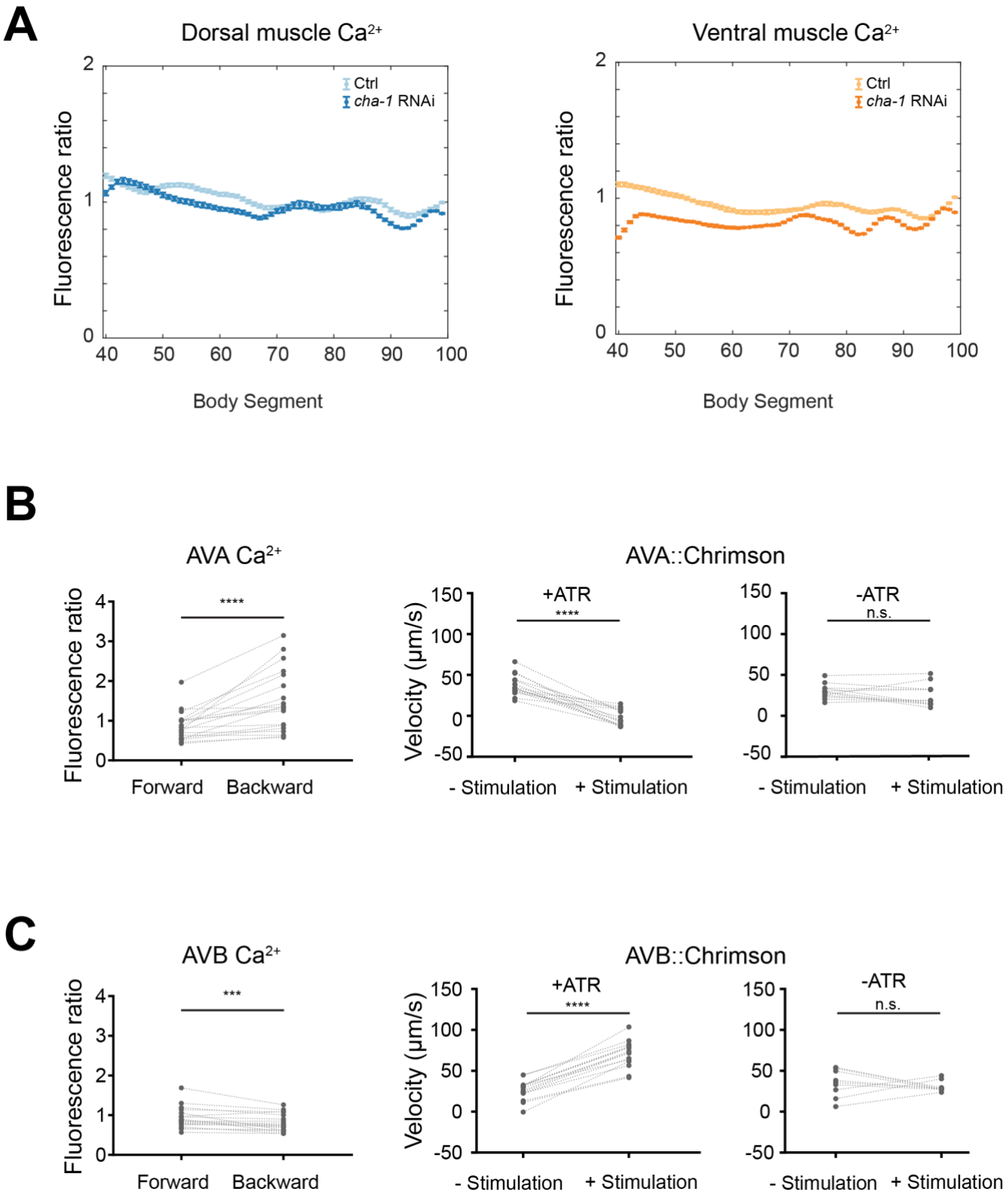
A
Dorsal muscle Ca2+
Ventral muscle Ca2+
Ctrl
cha-1 RNAi
Fluorescence ratio
Body Segment
B
AVA Ca2+
AVA::Chrimson
****
Forward
Backward
Velocity (µm/s)
+ATR
-ATR
n.s.
- Stimulation
+ Stimulation
C
AVB Ca2+
AVB::Chrimson
***

Figure S6. Effect of genetic and optogenetic manipulation of eINs in L1 larvae, related to Figure 6 (A) and Discussion (B, C).

(A) RNAi-mediated knockdown of *cha-1* in all eINs leads to stronger reduction of ventral muscle activity. Dorsal (left) and ventral (right) muscle calcium signals compared between larvae carrying only the calcium reporter (Ctrl) and larvae that carried an additional transgene expressing anti-sense *cha-1* in all eINs (*cha-1* RNAi). Segments 40-100 (instead of 33-100, as in Figure 6) constituted the body because these larvae were slightly younger. Related to Figure 6.

(B) (Left) The AVA eIN exhibited higher calcium activity during backward movement. n = 19 larvae. (Middle/right panels) Optogenetic activation of AVA led to reversals. Mean velocities during non-stimulated and stimulated phases were compared in the control group (-ATR) (n = 12 larvae) and the experimental group (+ATR) (n = 15 larvae). **** $p < 0.0001$. Related to Discussion.

(C) (Left) The AVB eIN exhibited higher calcium activity during forward movement (n = 19 larvae). *** $p = 0.0006$. (Middle/right panels) Optogenetic activation of AVB led to increased forward velocity. Control group (-ATR): n = 9 larvae. Experimental group (+ATR): n = 15 larvae. **** $p < 0.0001$. All p-values were calculated using the Wilcoxon matched-pairs signed rank test. Related to Discussion.

Supplemental References

S1. Butler, V.J., Branicky, R., Yemini, E., Liewald, J.F., Gottschalk, A., Kerr, R.A., Chklovskii, D.B., and Schafer, W.R. (2015). A consistent muscle activation strategy underlies crawling and swimming in Caenorhabditis elegans. J R Soc Interface *12*, 20140963.

S2. Pinan-Lucarre, B., Tu, H., Pierron, M., Cruceyra, P.I., Zhan, H., Stigloher, C., Richmond, J.E., and Bessereau, J.-L. (2014). C. elegans Punctin specifies cholinergic versus GABAergic identity of postsynaptic domains. Nature *511*, 466–470.

S3. Liewald, J.F., Brauner, M., Stephens, G.J., Bouhours, M., Schultheis, C., Zhen, M., and Gottschalk, A. (2008). Optogenetic analysis of synaptic function. Nat Methods *5*, 895–902.

S4. Schmitt, C., Schultheis, C., Husson, S.J., Liewald, J.F., and Gottschalk, A. (2012). Specific expression of channelrhodopsin-2 in single neurons of *Caenorhabditis elegans*. PLoS One *7*.